

RESEARCH ARTICLE

10.1029/2019JC015192

Key Points:

- Coastal upwelling influenced spatial and temporal patterns of Lake Erie hypoxia
- A physical dissolved oxygen model linked to a numerical ocean model exhibited useful skill
- Model bias in dissolved oxygen suggested an east-west gradient in sediment oxygen demand

Supporting Information:

- Supporting Information S1

Correspondence to:

M. D. Rowe,
mark.rowe@noaa.gov

Citation:

Rowe, M. D., Anderson, E. J., Beletsky, D., Stow, C. A., Moegling, S. D., Chaffin, J. D., et al. (2019). Coastal upwelling influences hypoxia spatial patterns and nearshore dynamics in Lake Erie. *Journal of Geophysical Research: Oceans*, 124, 6154–6175. <https://doi.org/10.1029/2019JC015192>






Received 16 APR 2019

Accepted 2 AUG 2019

Accepted article online 8 AUG 2019

Published online 24 AUG 2019

Coastal Upwelling Influences Hypoxia Spatial Patterns and Nearshore Dynamics in Lake Erie

M. D. Rowe¹ , E. J. Anderson¹ , D. Beletsky² , C. A. Stow¹ , S. D. Moegling³, J. D. Chaffin⁴ , J. C. May⁵, P. D. Collingsworth⁶ , A. Jabbari⁷, and J. D. Ackerman⁷ 

¹NOAA Great Lakes Environmental Research Laboratory, Ann Arbor, MI, USA, ²Cooperative Institute for Great Lakes Research, Ann Arbor, MI, USA, ³Cleveland Water, Cleveland, OH, USA, ⁴F.T. Stone Laboratory and Ohio Sea Grant, The Ohio State University, Columbus, OH, USA, ⁵Great Lakes National Program Office, U.S. Environmental Protection Agency, Chicago, IL, USA, ⁶Department of Forestry and Natural Resources and Illinois-Indiana Sea Grant, Purdue University, West Lafayette, IN, USA, ⁷Department of Integrative Biology, University of Guelph, Guelph, Ontario, Canada

Abstract Hypoxia, defined as dissolved oxygen (DO) < 2 mg/L, in the central basin of Lake Erie has been studied since the mid-1900s. Even so, spatial patterns of hypoxia, and episodic hypoxia in nearshore areas where drinking water plant intakes are located, are not well characterized owing to limited observations and short-term dynamics. We evaluated a physically based, DO model with respect to patterns of hypoxia observed in Lake Erie. The DO model used assigned rates of sediment and water column oxygen demand that were temperature dependent but otherwise spatially and temporally uniform. The DO model was linked to National Oceanic and Atmospheric Administration's (NOAA) Lake Erie Operational Forecasting System hydrodynamic model, an application of the Finite Volume Community Ocean Model (FVCOM). Model temperature and DO were compared with observations from ship-based studies, real-time sensor networks and an array of moored sensors that we deployed in 2017. In years with dominant southwesterly winds, persistent downwelling occurred along the south shore, which resulted in a thinner thermocline and earlier initiation of hypoxia along the south shore than the north. Occasional northeast winds temporarily reversed this pattern, causing upwelling along the south shore that brought hypoxic water to nearshore locations and water intakes. The DO model reproduced observed spatial and temporal patterns of hypoxia and revealed locations subject to episodes of hypoxia, including nearshore Ohio, north of Pelee Island, and near the Bass Islands. Model skill was limited in some respects, highlighting the importance of accurate simulation of the thermal structure and spatial patterns of oxygen demand rates.

Plain Language Summary Hypoxia, defined as dissolved oxygen (DO) < 2 mg/L, results from a combination of physical and biological processes. Hypoxia in Lake Erie reduces habitat and food supply for fish and complicates drinking water treatment. We applied a mathematical model that was driven by weather information (wind and air temperature) and simulated water temperature, currents, and DO. By evaluating whether a model that focused on physical processes could predict hypoxia, we investigated the relative importance of physical versus biological drivers. We compared model temperature and DO with measurements conducted by us and by others. In years with dominant southwesterly winds, persistent downwelling occurred along the south shore, which resulted in a thinner thermocline and earlier initiation of hypoxia along the south shore than the north. Occasional northeast winds temporarily reversed this pattern, causing upwelling along the south shore that brought hypoxic water to nearshore locations and water intakes. The DO model reproduced observed spatial and temporal patterns of hypoxia, indicating the importance of physical drivers, and revealed locations subject to episodes of hypoxia, including nearshore Ohio, north of Pelee Island, and near the Bass Islands.

1. Introduction

Coastal upwelling occurs when wind stress is oriented parallel to the coast, inducing an offshore upper layer transport (Ekman transport), resulting in upward displacement of deep water in a density stratified system. Persistent upwellings occur along the eastern boundaries of the Atlantic and Pacific basins owing to persistent equatorward winds east of subtropical highs (Wang et al., 2015). In other regions, episodic upwelling or downwelling occurs when passing fronts cause along-shore winds that persist for several days (Rodrigues & Lorenzetti, 2001). Coastal upwellings have important ecological

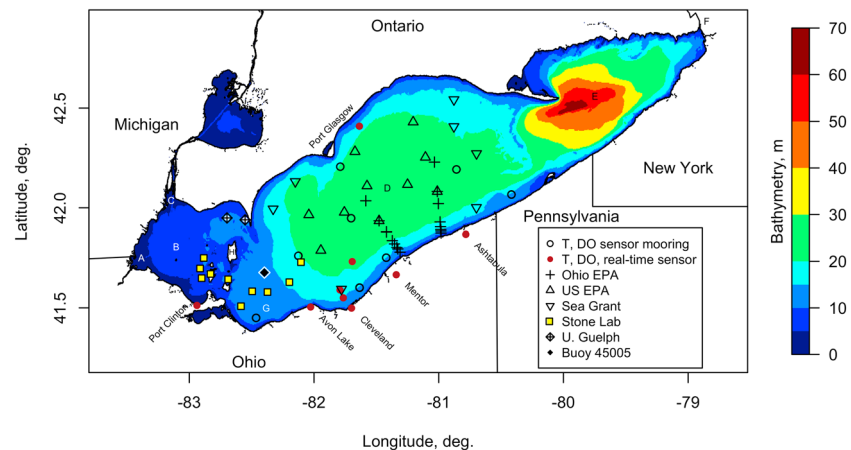


Figure 1. Geographic location and bathymetry of Lake Erie, showing bordering U.S. states and the Canadian province of Ontario. Geographic features include (A) Maumee Bay, (B) western basin, (C) Detroit River, (D) Central basin, (E) Eastern basin, (F) Niagara River, (G) Sandusky basin, and (H) Pelee Island. Symbols indicate the locations of observational data collection.

consequences, drawing cold, nutrient rich, and in some cases oxygen depleted waters into the coast (Wang et al., 2015).

The Laurentian Great Lakes, located along the United States-Canada border in eastern North America, are sufficiently large to experience Ekman transport-driven coastal upwelling dynamics similar to the coastal ocean (Beletsky et al., 1997). The Great Lakes have horizontal scales of tens to hundreds of kilometers, compared to internal Rossby radius of deformation of 3–5 km (Csanady, 1984; Rao & Schwab, 2007). The central basin of Lake Erie is 80-km wide and 190-km long with a mean depth of ~20 m (Figure 1). Persistent upwelling along the north coast of the central basin, driven by Ekman transport associated with frequent winds from the southwest, was reported from surveys of lake thermal structure from the 1920s through 1960s (Mortimer, 1987) and in more recent studies (Bartish, 1987; Bouffard et al., 2012; Rao et al., 2014). Beletsky et al. (2012) pointed to surface water convergence driven by anticyclonic vorticity in the surface wind (Ekman pumping) to explain the observed bowl-shaped thermocline in the central basin. Thus, Ekman transport has an important influence on thermal structure and circulation in the central basin of Lake Erie.

Despite marked recovery of conditions following implementation of legislation in the USA and Canada in the 1970s to limit loading of the limiting nutrient phosphorus into the lake, Lake Erie has become increasingly eutrophic since the early 2000s with issues of hypoxia and harmful algal blooms reemerging as dissolved phosphorus loads to the lake have increased (Scavia et al., 2014; Watson et al., 2016). Hypoxia is detrimental to ecosystem services provided by Lake Erie, including economic and culturally important fishery and tourism (Allan et al., 2015). In addition, drinking water treatment plants drawing water from the Ohio coast of the central basin serve 1.8 million people (<https://epa.ohio.gov>; accessed 2018-5-4). Rapid changes in bottom DO occur in coastal areas, caused by upwelling or internal waves that result in shoreward advection of hypoxic bottom water. These dynamics can alter fish distribution, cause fish kills, or cause rapid changes in water quality at drinking water plant intakes (Kraus et al., 2015; Rao et al., 2014; Ruberg et al., 2008).

Spatial patterns of hypoxia, and episodes of hypoxia in nearshore areas where drinking water intakes are located, are not well characterized owing to limited observations of bottom dissolved oxygen (DO) and dynamic movement of the hypoxic boundary in nearshore areas. Hypoxia in Lake Erie has been monitored routinely by ship-base surveys since the 1980s (Zhou et al., 2013) and earlier episodic surveys (Britt, 1955; Burns, 1976). Most of these surveys have, however, focused on the deepest waters of the central basin (>20 m) and were not designed to establish the coastal boundaries of the hypoxic area. Recent studies have documented hypoxia in shallower locations (~12-m depth) not included in long-term monitoring (Perello et al., 2017). In addition, monthly ship-based surveys lack the temporal resolution needed to detect short-

term dynamics. Model simulations have predicted initiation of hypoxia in relatively shallow coastal areas prior to deeper locations in the central basin, although these results were not confirmed with observations (Bocaniov et al., 2016). In the past 5 years, DO sensors have been deployed in many locations that were not routinely monitored previously, providing new opportunities to visualize the spatial and temporal extent of hypoxia and assess models (e.g., <https://portal.glos.us/>).

Mechanistic models of DO dynamics and hypoxia vary widely in complexity, and an appropriate level of complexity should be selected, depending on the goal of a specific study. Models are more likely to produce useful predictions when there are strong physical, as opposed to chemical or ecological, drivers (Arhonditsis et al., 2006; Robson, 2014). We identify two general categories of DO models that we refer to as (1) biophysical and (2) physical. A biophysical DO model may represent biological production of labile organic matter using multiple nutrient, plankton, and organic carbon state variables, whereas a physical DO model may use only a few physical state variables (temperature and DO) with prescribed rates of oxygen demand. For example, spatially resolved physical DO models showed reasonable skill in simulating both short-term and seasonal hypoxia dynamics in Chesapeake Bay (Li et al., 2015; Scully, 2013), whereas a more complex biophysical DO model produced greater spatial and temporal variability in DO than the physical DO models, but with similar skill (Bever et al., 2013). Another noteworthy physical DO model was the one-dimensional, vertical model of Rucinski et al. (2010), which exhibited reasonable skill in simulating interannual variability of hypoxia in Lake Erie.

The present study was motivated by the hypothesis that spatial and temporal patterns of hypoxia in Lake Erie, including episodes (less than a few days) of nearshore hypoxia, can be explained primarily by physical processes without accounting for spatial and temporal variation in sediment and water column oxygen demand associated with biological production of labile organic matter. Our approach is to use a three-dimensional, spatially resolved hydrodynamic model linked to a physical DO model that uses temperature-dependent but otherwise spatially and temporally uniform assigned rates of sediment and water column oxygen demand.

2. Methods

2.1. Hydrodynamic Model

The FVCOM is an unstructured grid, finite-volume, free surface, three-dimensional primitive equation ocean model that solves the momentum, continuity, temperature, salinity, and density equations (Chen et al., 2003). Turbulence closure is implemented through the MY-2.5 scheme for vertical mixing (Galperin et al., 1988), and the Smagorinsky scheme for horizontal mixing (Smagorinsky, 1963).

FVCOM has been adapted and implemented for the Great Lakes in several recent studies (Anderson et al., 2010; Anderson et al., 2015; Anderson & Schwab, 2013; Bai et al., 2013). The FVCOM application developed for the Lake Erie Operational Forecast System (LEOFS) was applied in this study (Anderson et al., 2018; Kelley et al., 2018). Bathymetry was interpolated from the NOAA National Geophysical Data Center (www.ngdc.noaa.gov/mgg/greatlakes/greatlakes.html). The unstructured grid consisted of 6,106 nodes and 11,509 elements. Spatial resolution was typically 2 km midlake, transitioning to 0.5 km at the coast, with 20 uniform vertical sigma layers. The grid was refined in regions of interest, including 1.5 km in the western basin and 0.5 km in Maumee Bay and the islands (Figure 1; locations D, B, A, and H).

We generated atmospheric forcing conditions using station-based interpolation methods, as in the NOAA Great Lakes Coastal Forecasting System (Beletsky et al., 2003; Schwab & Beletsky, 1998). Hourly meteorological forcing variables of wind speed, wind direction, air temperature, dew point temperature, and cloud cover were interpolated over Lake Erie from 42 meteorological stations and additional offshore NOAA/National Data Buoy Center buoys (45004, 45132, and 45142; www.ndbc.noaa.gov), when available. Wind speeds were adjusted to 10-m height and empirical relationships were used to adjust land-based meteorological variables for over-lake modification (Beletsky et al., 2003; Schwab & Beletsky, 1998). We conducted hindcast simulations for 2006, the year of the upwelling event described by Ruberg et al. (2008), and 2010–2017, recent years with an abundance of observational data. We ran daily nowcast/forecast simulations in 2017 using interpolated forcing for the 24-hr nowcast simulation and a meteorological forecast from the National Digital Forecast Database (www.ncdc.noaa.gov) for the 10-day forecast simulation. In addition

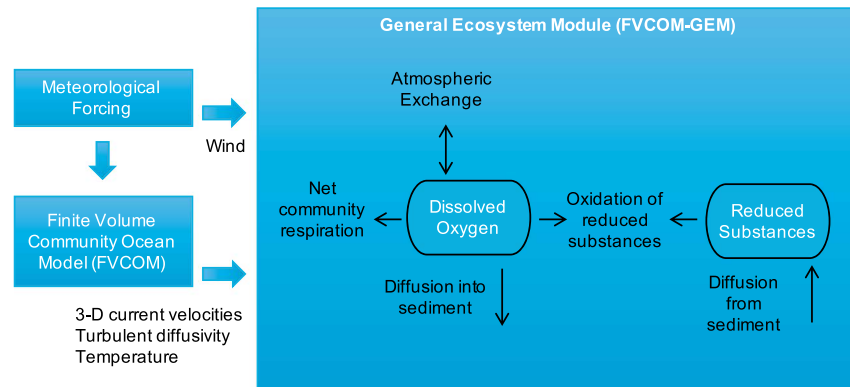


Figure 2. Process diagram for the physical dissolved oxygen model, showing model state variables (ovals), oxygen budget processes (arrows), and data linkage to FVCOM and meteorological forcing (block arrows). GEM = General Ecological Module.

to interpolated forcing, we also evaluated atmospheric forcing from the NOAA High-Resolution Rapid Refresh (HRRR) model to determine model sensitivity to model-derived versus interpolated wind fields. HRRR is a weather forecasting atmospheric model that assimilates observational data from many sources (Benjamin et al., 2016; <https://rapidrefresh.noaa.gov/hrrr/>). We conducted hindcast simulations with HRRR model forcing for 2016 and 2017.

2.2. DO Model

The FVCOM General Ecological Module (GEM) is a generalized biological module that allows users to select from several prebuilt biological models or construct their own model by specifying any number of state variables of functional types including nutrients, phytoplankton, zooplankton, detritus, or bacteria (Chen et al., 2013; Ji et al., 2008). The model state variables are subject to three-dimensional advection and diffusion using the same numerical methods and unstructured computational grid as for scalars (e.g., temperature and dissolved and particulate constituents) in FVCOM (Chen et al., 2003). Scalar variables are determined at each node of the model grid by tracking a net flux through the flow faces of a roughly hexagonal tracer control element (Chen et al., 2003) that is divided into a specified number of terrain-following σ layers (20 in our case). We used the GEM code that is part of the standard FVCOM code distribution (v3.2.0; <http://fvcom.smast.umassd.edu/>, accessed 2015-4-14) and is executed concurrently with the hydrodynamic code and integrated on the same time step (~10 s).

Building on the flexible GEM framework, we defined a model having two state variables: DO and reduced substances (Figure 2), following the conceptual approach of Müller et al. (2012). The reduced substances state variable, O_{2e} , represents reduced substances, such as methane (CH_4) and ammonium (NH_4^+), which are released from the sediment and accumulate after hypolimnetic O_2 depletion, as oxygen equivalents (the amount of oxygen that would be consumed by the reduced substances when oxidized in the presence of DO). The change of these state variables over time in a single tracer control element (omitting advection and turbulent diffusion terms) was given as

$$\frac{d}{dt} O_2 = F_a \frac{A_a}{V_{\text{TCE}}} - F_{\text{sed}} \frac{A_s}{V_{\text{TCE}}} - R_{\text{red}} - R_{\text{wcod}} \quad (1)$$

$$\frac{d}{dt} O_{2e} = F_{\text{red}} \frac{A_s}{V_{\text{TCE}}} - R_{\text{red}} \quad (2)$$

Symbols are defined in Table 1.

The air-water exchange flux of oxygen, F_a , was calculated as

$$F_a = k_a(O_{2s} - O_2) \quad (3)$$

The DO concentration at equilibrium with the atmosphere, O_{2s} , was calculated as a function of temperature at zero salinity (Greenberg et al., 1989). The air-water transfer velocity for oxygen, k_a , was calculated as the

Table 1
Model Variables and Parameters

Symbol	Definition
t	time
O_2	Dissolved oxygen (DO) concentration
O_{2s}	DO concentration at equilibrium with the atmosphere
O_{2e}	Reduced substances as oxygen equivalent concentration
V_{TCE}	Volume of tracer control element (TCE)
A_a	Area of air-water interface bordering the TCE
A_s	Area of sediment-water interface bordering the TCE
F_a	Air-water exchange flux of DO
$F_{sod}; F_{sod_ref}$	Flux of DO into the sediment; at T_{ref}
F_{red}	Flux of reduced substances from sediment
R_{red}	Reaction rate of DO with reduced substances
$R_{wcod}; R_{wcod_ref}$	Rate of water column oxygen demand (net community respiration); at T_{ref}
k_a	Air-water exchange gas transfer velocity for DO
k_{aw}	Wind speed-dependent k_a
k_{ac}	Shallow-water current-dependent k_a
U_{10}	Wind speed at 10-m height
S_c	Schmidt number for DO in water
$\theta_{wcod}, \theta_{sod}, \theta_e$	Temperature-dependence parameter
T_{ref}	Reference temperature for oxygen demand rates (20 °C)
T_w	Water temperature
k_e	Rate constant for oxidation of reduced substances
K_{he}	Half-saturation constant for oxidation of reduced substances

maximum of the values calculated for current interaction with bottom roughness, k_{ac} , in areas of shallow bathymetry using empirical functions (Chapra, 1997; their Figure 20.7) or wind-driven turbulence, k_{aw} , in areas of deep bathymetry (Wanninkhof et al., 2009; their equation 37), with the latter being the dominant process:

$$k_a = \max(k_{ac}, k_{aw}); k_{aw} \left[\frac{cm}{h} \right] = 0.24U_{10}^2 \left(\frac{S_c}{660} \right)^{-0.5} \quad (4)$$

The temperature-dependent Schmidt number for oxygen in water was calculated after Johnson (2010).

The flux of DO into the sediment was calculated as a spatially uniform assigned value with temperature dependence

$$F_{sod} = F_{sod_ref} \theta_{sod}^{(T_w - T_{ref})} \quad (5)$$

More complex expressions are available for F_{sod} . For example, we also evaluated the model of Higashino (2011), which gave F_{sod} as a function of DO in the overlying water, bottom current velocity, diffusivity, and reaction rate in the sediment. We found that either expression could be calibrated to minimize the bias in predicted bottom DO, but the more complex model for F_{sod} did not improve skill metrics for spatiotemporal variation in bottom DO in our sensitivity trials, so we used the simpler equation (5).

Müller et al. (2012) synthesized long-term observations of hypolimnetic oxygen depletion across eutrophic lakes in Europe of differing depth and found that a simple model could predict the areal hypolimnetic mineralization rate (AHM) as a function of hypolimnion thickness alone,

mainly because settling organic matter had more time to decompose in the water column of deeper lakes. AHM is equal to the rate of DO depletion in the presence of oxygen (sediment oxygen demand) and also includes accumulated reduced substances released from the sediment after DO depletion (Müller et al., 2012). An estimate of AHM for Lake Erie can be obtained from Figure 1 of Müller et al. (2012), following their assumed surface mixed-layer depth of 10 m and the mean depth of Lake Erie central basin of 20 m; applying the resulting hypolimnion thickness of 10 m to their Figure 1 results in an AHM of $0.7 \text{ gO}_2 \cdot \text{m}^{-2} \cdot \text{d}^{-1}$. Rucinski et al. (2010) used a sediment oxygen demand value of $0.7 \text{ gO}_2 \cdot \text{m}^{-2} \cdot \text{d}^{-1}$ in their model, based on a literature review of values measured in the Lake Erie central basin, which is identical to the value we obtained from the simple model of European eutrophic lakes of Müller et al. (2012). Müller et al. (2012) further divided AHM into two components: (1) the mineralization of freshly settled organic matter and (2) reduced substances released from the anoxic sediment (e.g., methane, ammonium, reduced iron, and manganese), with the latter F_{red} having a relatively constant value across eutrophic lakes of $\sim 0.36 \text{ gO}_{2e} \cdot \text{m}^{-2} \cdot \text{d}^{-1}$. Following the calibrated model of Rucinski et al. (2010) for Lake Erie, and consistent with the estimate from Müller et al. (2012), we set $F_{red} = 0.36 \text{ gO}_{2e} \cdot \text{m}^{-2} \cdot \text{d}^{-1}$ and $F_{sod_ref} = 0.34 \text{ gO}_2 \cdot \text{m}^{-2} \cdot \text{d}^{-1}$, resulting in a total rate of sediment oxygen demand of $0.7 \text{ gO}_2 \cdot \text{m}^{-2} \cdot \text{d}^{-1}$ at T_{ref} , and we set a net community respiration rate in the water column,

$$R_{wcod} = R_{wcod_ref} \theta_{wcod}^{(T_w - T_{ref})} \quad (6)$$

with $R_{wcod_ref} = 0.03 \text{ gO}_2 \cdot \text{m}^{-3} \cdot \text{d}^{-1}$ (Rucinski et al., 2010; their Figure 14) and $\theta_{wcod}, \theta_{sod} = 1.04$. The concentration of DO in the model was constrained to be ≥ 0 . In the eastern basin (Figure 1), F_{red} , F_{sod_ref} , and R_{wcod_ref} were reduced by half to produce summer DO minimum matching observations from U.S. Environmental Protection Agency (USEPA); however, the eastern basin was not included in our skill assessment.

Finally, we specified a reaction rate for oxidation of reduced substances in the presence of oxygen, which consumed both reduced substances and oxygen, after Cerco and Noel (2004):

$$R_{\text{red}} = O_{2e} k_e \theta_e^{(T_w - T_{\text{ref}})} \frac{O_2}{(O_2 + K_{\text{he}})} \quad (7)$$

with $k_e = 20 \text{ d}^{-1}$, $\theta_e = 1.042$, and $K_{\text{he}} = 0.5 \text{ gO}_2/\text{m}^3$.

We initialized DO model simulations on 1 April of each year with DO set at equilibrium with the atmosphere and reduced substances set to zero. We initialized temperature and currents from the corresponding LEOFS nowcast daily simulation. LEOFS was first initialized on 1 January 2004 with uniform temperature of 2 °C, and daily nowcast simulations were run sequentially after using interpolated meteorological forcing. Dynamic water levels (6 min) were prescribed at the open boundaries at Detroit and Niagara Rivers, taken from adjustments to the NOAA/National Ocean Service gauges at Gibraltar (9044020) and Buffalo (9063020), to drive the primary inflow and outflow, respectively (Figure 1; locations C and F). We prescribed incoming temperature at the Detroit River from gauge data, set DO at saturation, and reduced substances at zero.

2.3. Observations

We deployed a network of eight taught-line moorings with temperature and DO sensors at 4–5 levels in the central basin in May–October of 2017 (Figure 1). Four moorings were located along the Ohio coast in 12- to 14-m depth to capture upwelling/downwelling dynamics along the edge of the hypoxic zone. An additional four moorings were located at the center and along north-south and east-west axes of the central basin to capture basin-scale dynamics. We focus on the bottom sensor data (PME miniDOT: Temp resolution 0.0001 °C, accuracy 0.002 °C; DO resolution 0.01 mg/L, accuracy $\pm 5\%$).

We gathered additional temperature and DO sensor data from multiple sources. In May to October of 2014–2016, U.S. Environmental Protection Agency Great Lakes National Program Office and Illinois-Indiana Sea Grant deployed near-bottom sensors at ~ 17 locations to resolve spatial patterns of hypoxia (Figure 1). Starting in 2016, the Great Lakes Observing System and LimnoTech deployed real-time sensors at drinking water intakes and three mooring locations (Figure 1; <https://portal.glos.us/>). The province of Ontario deployed a sensor mooring near Port Glasgow (Figure 1; <http://ontario3.loboviz.com/>). Sensors in the pump stations of drinking water intakes (Figure 1) were exposed to bottom water collected within 0.5 km of the coast (Port Clinton, Avon Lake, Mentor, Ashtabula) or 5 km from the coast (Cleveland). From 2008 to 2016, NOAA Great Lakes Environmental Research Laboratory maintained a real-time near-bottom sensor at the 20-m depth location ~ 25 km north of Cleveland (Figure 1). University of Guelph deployed moored temperature and DO sensors at two locations north of Pelee Island (Figure 1), 24 August to 17 September 2017 (Jabbari et al., 2019). Wind data were obtained from the National Data Buoy Center (Figure 1; Buoy 45005; <https://www.ndbc.noaa.gov/>, accessed 2016-9-21).

Vertical profiles of temperature and DO in the water column collected in ship-based surveys were obtained from several sources (referred to as conductivity, temperature, depth, or CTD profiles). USEPA conducted monthly surveys (July to October) in each hindcast year at 10 deep-water stations in the central basin (Figure 1). Ohio Environmental Protection Agency conducted surveys approximately monthly in four transects from the Ohio coast to midlake (Figure 1). The Ohio State University Stone Lab conducted surveys on several occasions in the western and Sandusky basins (Figure 1).

2.4. Model Skill Statistics

We evaluated model skill in simulating bottom temperature and DO using conventional skill metrics defined by Stow et al. (2009) including the mean bias, correlation coefficient, root-mean-square error, and modeling efficiency (Nash-Sutcliffe efficiency, NS). Accurate simulation of surface mixed-layer thickness (epilimnion) and hypolimnion thickness are important in a hypoxia model. Modeled and observed temperature profiles do not have distinct boundaries for these layers. To obtain values of layer thickness for skill assessment, we approximated modeled and observed temperature profiles with an idealized three-layer structure (least squares fit) having uniform temperature in the epilimnion and hypolimnion, and a linear temperature gradient in the metalimnion (Beletsky et al., 2006). Fitting the three-layer structure yields four parameters: the temperature and thickness of the epilimnion and hypolimnion.

In addition, we evaluated model skill in predicting low DO and rapid temperature decrease events at drinking water intakes using skill statistics for binary events, following Hogan and Mason (2012). We calculated

the Pierce Skill Score (PSS) from the elements of the contingency table, which are the number of a , correctly predicted events (hits); b , false events (false alarms); c , false negatives (misses); and d , correct nonevents. The PSS gives the hit rate, $a/(a + c)$ minus the false alarm rate, $b/(b + d)$.

$$\text{PSS} = \frac{ad - bc}{(b + d)(a + c)} \quad (8)$$

PSS values range from -1.0 to 1.0 , with positive values indicating that the hit rate was greater than the false positive rate, and therefore, the model had greater skill than a random forecast or constant event or nonevent prediction (Hogan & Mason, 2012). To provide a reference forecast for skill comparison, we defined a *persistence* forecast as the assumption of no change from the most recent real-time sensor observation, which represents the best available information to a forecast user in the absence of a useful model.

3. Results

3.1. Spatial and Seasonal Patterns of Hypoxia

Hypoxia initiated in July in a relatively narrow band along the Ohio coast prior to becoming established in the midcentral basin and along the Ontario coast in most hindcast years. For example, July 2016 monthly mean DO was <2 mg/L at 2 sensors within 10 km north of Cleveland, while 11 sensors located further north were > 2 mg/L, with one exception, generally consistent with simulated bottom DO and temperature (Figure 3). A similar pattern was simulated and observed in July 2017, when five sensors were available near the Ohio coast showing hypoxia, while sites further north were not hypoxic (Figure 4). Among the hindcast years, a similar pattern of hypoxia initiation in July along the Ohio coast occurred in model simulations of 2006, 2010, 2011, 2014, 2016, and 2017, while the timing of hypoxia initiation along north and south coasts was similar in 2012, 2013, and 2015 (Figures S1–S7 in the supporting information). Sensors at pump stations of drinking water plants with bottom water intakes located 0.5–1 km offshore near Avon Lake, Mentor, and Ashtabula were shoreward of the location where the thermocline intersected the bottom, and therefore sampled relatively warm, normoxic water of the surface mixed layer (Figures 3 and 4), with the exception of upwelling events.

Hypoxia occurred frequently in July and August in the Sandusky basin, and in the western basin north of Pelee island, regions of intermediate depth between that of the western basin (~ 8 -m mean) and central basin (~ 20 -m mean). Mean DO in July was hypoxic in the Sandusky basin in eight of nine hindcast simulations, while hypoxia occurred north of Pelee Island in four of nine hindcast simulations. Ship-based surveys in 2013–2017 and our sensor mooring in 2017 provided observations for model assessment in the Sandusky basin. Simulated hypoxia in the Sandusky basin was relatively unbiased in June, July, and August but retained hypoxic conditions longer than observed in September and October (Figure 5), and overall skill was moderate (Bias 0.75 °C, -0.77 mgO₂/L; NS temp. 0.69 , NS DO 0.24). Few observations were available to assess the model north of Pelee Island, with the exception of the University of Guelph moorings (Jabbari et al., 2019) deployed from 24 August to 17 September 2017 (Figure 5); bottom temperature and DO were biased high (2.4 °C, 1.4 mgO₂/L) and moderately correlated (0.41 , 0.81 , respectively) over this limited time period, suggesting that the simulated surface mixed layer was in contact with the bottom to a greater extent than observed.

In late August through October of the hindcast years, hypoxia gradually retreated from shallower to deeper regions as the seasonal deepening of the surface mixed layer re-aerated the lake to increasingly greater depths. Simulated and observed hypoxia in the Sandusky basin and north of Pelee Island ended in September or early October, earlier than in deeper parts of the central basin (Figures 3, 4, and S1–S7). In September, the center of the central basin was hypoxic in all hindcast years, while in October hypoxia retreated to isolated pockets in the deepest parts of the central basin or was not present (Figures 3, 4, and S1–S7).

There was a noteworthy temporary reversal of this seasonal pattern in August–September of 2017, when hypoxia reemerged in shallow areas. In August 2017, a period of relatively cool, windy weather caused deepening of the surface mixed layer and retreat of hypoxia to the deepest waters of the central basin. This pattern was reflected in the model and observations on 13 September, although the model overpredicted the

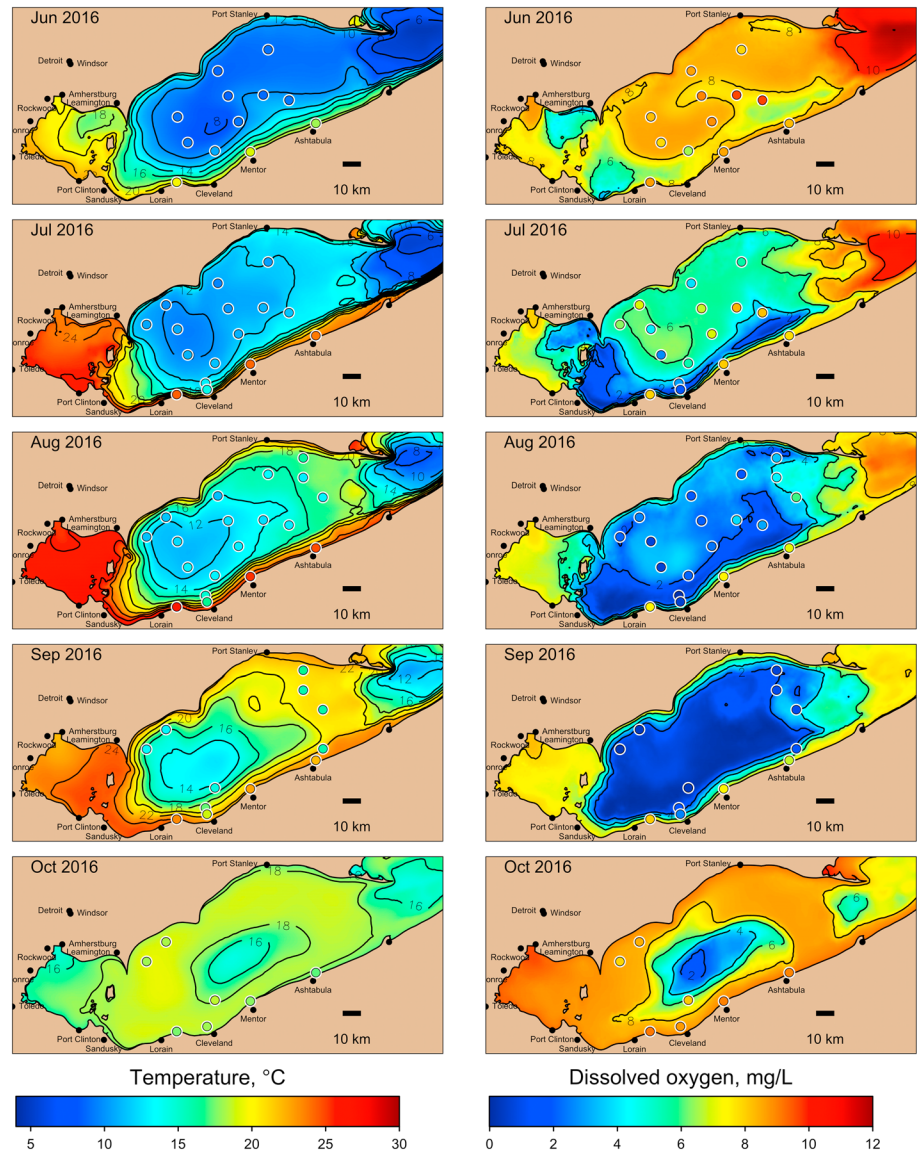


Figure 3. Monthly mean Lake Erie bottom temperature and dissolved oxygen for the 2016 hindcast simulation with interpolated meteorology. The same color scale is used for model data (color fields and contours) and observations (symbols).

extent of hypoxia on 25 August (Figure 5). By 25 September, a period of hot, calm weather had caused stratification and hypoxia to develop again in coastal waters of the central basin, and hypoxia was observed at two locations in the western basin (Figure 5). The model simulated this decrease of DO in coastal waters of the central basin and in the western basin (Figure 5; 9–25 vs 9–13), although observed DO was lower than simulated in some locations. At buoy 45005, the wind speed was 2.3 to 3.8 m/s (interquartile range) from 22 August to 12 September, and water surface temperature decreased from 23.7 to 19.6 °C, while wind speed was 1.0 to 2.0 m/s from 12 to 26 September, and the water temperature increased from 19.6 to 24.4 °C (Figure S8); this warming was sufficient to restratify the water column and cause redevelopment of hypoxia (or near hypoxia) in shallow areas throughout the central and western basins.

Over the nine hindcast years, more than 10,000 daily mean observations of bottom temperature and DO were available for model skill assessment (Table S1 and Figure 6), with extensive spatial and temporal coverage (Figures 1, 3–5, and S1–S7). Bottom temperature and DO were simulated with moderate skill (Table S1; NS 0.67, 0.51, respectively). Low magnitude of bias in simulated bottom DO (−0.36 vs

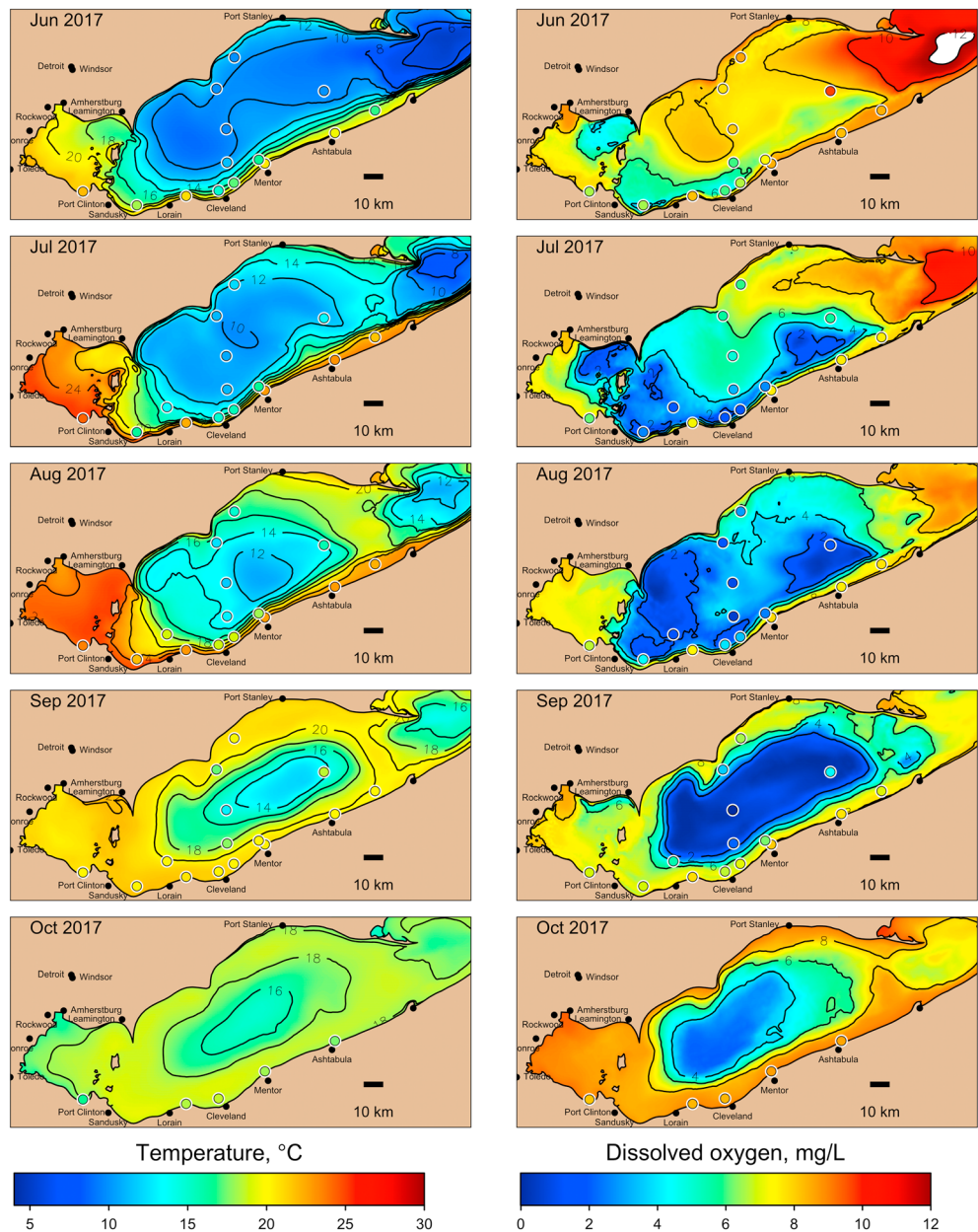


Figure 4. Same as Figure 3 but for 2017.

observed mean of $5.45 \text{ mgO}_2/\text{L}^1$) indicates that a reasonable rate of sediment oxygen demand was assigned based on literature values (Müller et al., 2012; Rucinski et al., 2010), while strong correlation (0.85 temp., 0.74 DO) indicated that spatial and temporal patterns of bottom temperature and DO were reasonably approximated by the model. In comparison to our Sandusky basin mooring and the Sandusky and western basin observations from Stone Lab (Figures 1 and 5), bottom temperature was simulated with greater skill than DO (NS 0.69, 0.24, respectively), mean bias was small in magnitude (0.75 vs observed mean of 17.72 C ; -0.77 vs observed mean of $4.73 \text{ mgO}_2/\text{L}$), and correlation was moderate (0.87 temp.; 0.62 DO). There was some tendency for overprediction of hypoxia in the Sandusky basin (Figure S9), especially in September–October (Figure 5), suggesting that deepening of the mixed layer in late summer was delayed in the model.

Accurate simulation of the thermocline location and thickness of the hypolimnion are important for a hypoxia model (Müller et al., 2012). A collection of more than a thousand high-resolution CTD profiles

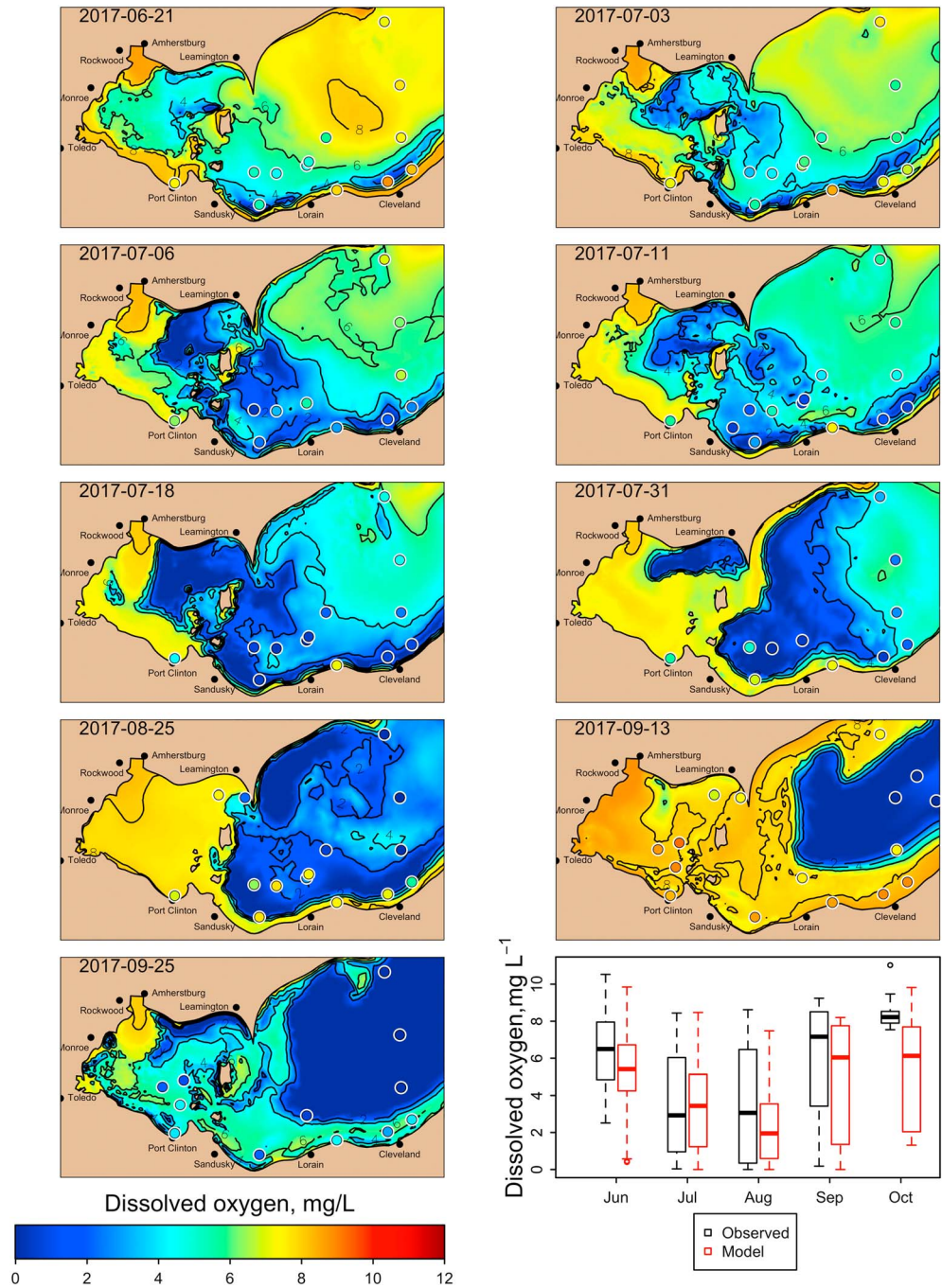


Figure 5. Daily mean Lake Erie dissolved oxygen on dates in 2017 when Stone Lab observations in Sandusky basin were available. The same color scale is used for model data (color fields and contours) and observations (symbols). The boxplot shows DO by month (observation, black; model, red) over 2013–2017 Stone Lab stations in Sandusky basin, islands, and western basin and our mooring in Sandusky basin. University of Guelph observations are shown on 25 August and 13 September north of Pelee Island. DO = dissolved oxygen.

provided for a rigorous assessment of the modeled vertical profiles of temperature and DO (Figure 6 and Table S1). Modeled surface mixed layer and hypolimnion thickness were correlated to observed values (0.53 SML, 0.65 hypolimnion thickness) but were biased thinner and thicker than observed values, respectively (−2.97 and 0.76 m). The opposing biases are a result of the modeled thermocline being more diffuse than observed, resulting in a metalimnion that is too thick.

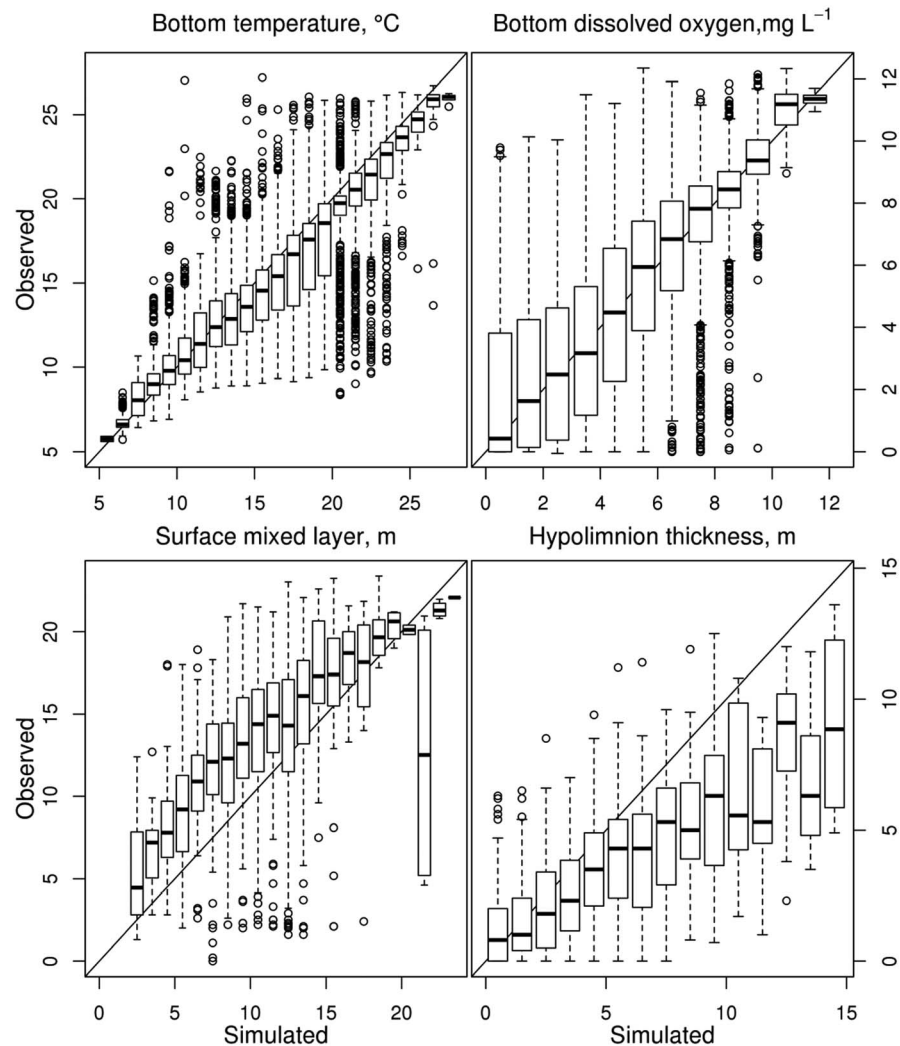


Figure 6. Comparison of simulated to observed Lake Erie bottom temperature and dissolved oxygen (daily mean), surface mixed layer, and hypolimnion thickness (hourly values) for hindcast simulations of 2006 and 2010–2017 with interpolated meteorology. Boxplots give the median and interquartile range with whiskers extending to 1.5 times the interquartile range and points beyond the whiskers plotted individually.

To test the assumption of spatially uniform sediment oxygen demand that was built into the model, we assessed spatial bias in simulation of bottom DO. The USEPA stations were selected for this purpose because there is a relatively long time series of monthly observations at a fixed set of 10 stations, all at >20-m depth in the central basin. Averaged over the nine hindcast simulations, there was a west-east trend in model bias for bottom DO, but the same trend was not apparent for hypolimnion thickness (Figure 7). Linear regression of bias versus longitude at the USEPA stations gave a highly significant slope for DO ($p < 0.001$) but a much less significant trend for temperature ($p = 0.07$) and for hypolimnion thickness ($p = 0.25$); results of this analysis were similar for the 2016–2017 HRRR simulations, although p values were larger owing to a smaller number of observations ($p = 0.02, 0.96, \text{ and } 0.86$ for temperature, DO, and hypolimnion thickness, respectively). Such a pattern could be indicative of a west-east gradient in central basin sediment and water column oxygen demand that was not represented in the model, which is consistent with the known west-east trophic gradient in Lake Erie from the eutrophic western basin to the oligotrophic eastern basin. Lack of an east-west trend for bottom temperature and hypolimnion thickness suggests that the trend in bottom DO bias was not explained by bias in these variables.

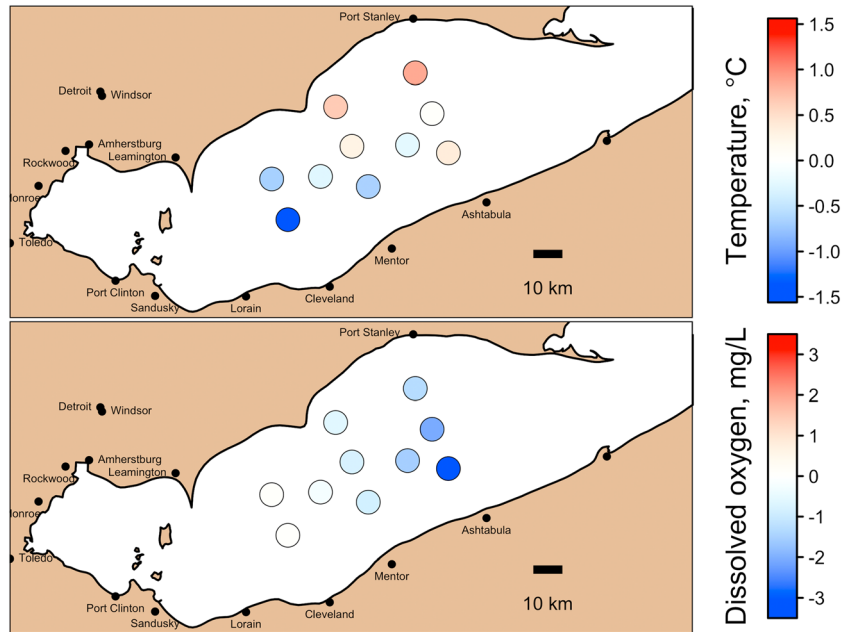


Figure 7. Spatial pattern of mean bias in bottom dissolved oxygen at USEPA stations for hindcast simulations of 2006 and 2010–2017 with interpolated meteorology. Positive bias indicates model values greater than observed. USEPA = U.S. Environmental Protection Agency.

3.2. Coastal Upwelling

Hypoxia initiation along the Ohio coast in July occurred for years in which June–July winds were more frequent from the southwest quadrant than from the northeast (Figure 8), directions roughly parallel to the long axis of the lake (Figure 1). For years in which hypoxia initiated at approximately the same time along

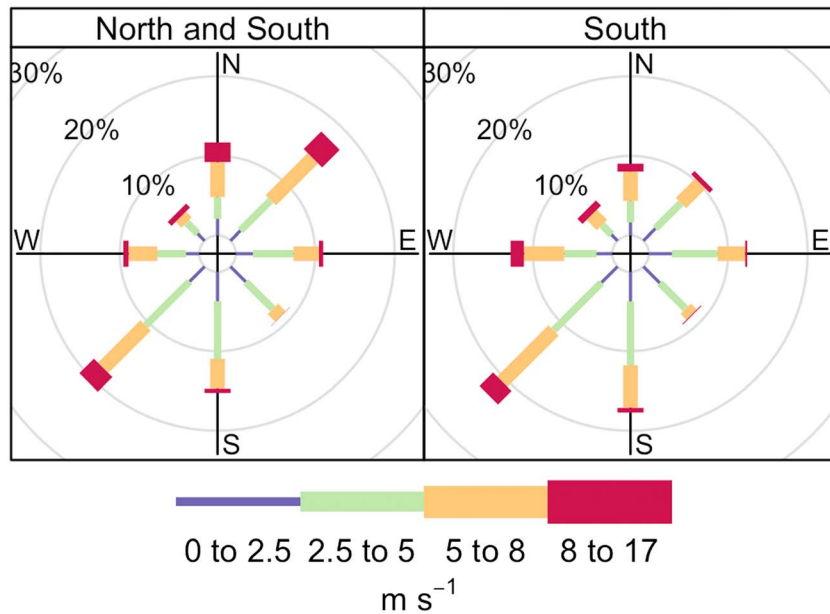


Figure 8. Wind rose plot showing frequency of June–July hourly winds at buoy 45005 (Figure 1) by direction and speed for hindcast simulation years in which hypoxia initiated first along the Ohio coast *South* (2006, 2010, 2011, 2014, 2016, and 2017), which was associated with more frequent SW versus SE winds in comparison to years in which hypoxia initiated equally along *South and North* coasts (2012, 2013, and 2015).

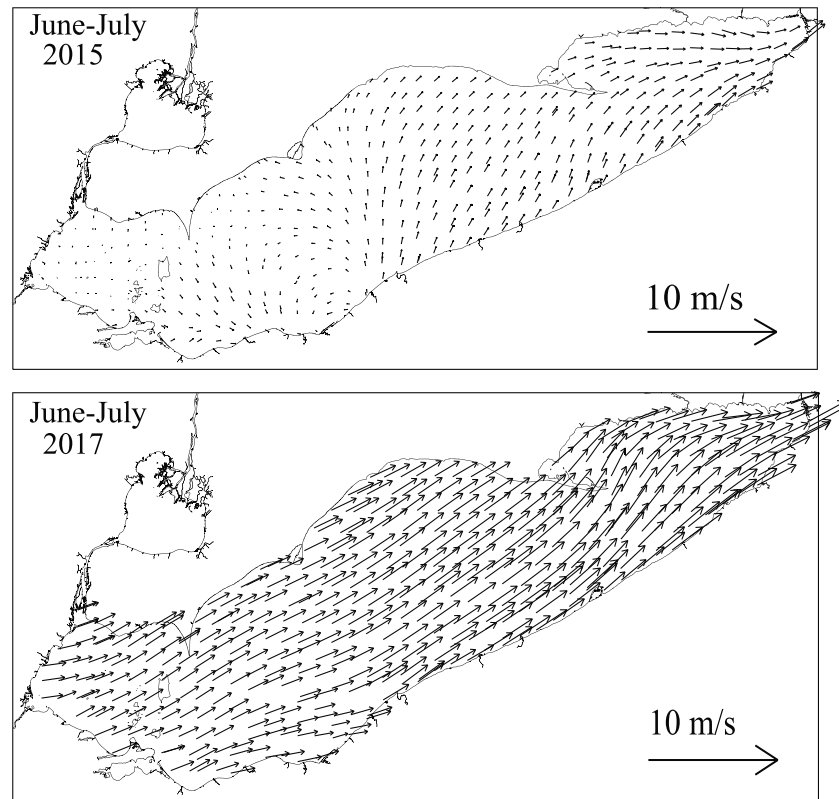


Figure 9. Mean June–July wind field in 2015 and 2017, interpolated from observations (see section 2).

the Ohio and Ontario coasts in July (2012, 2013, and 2015), the ratio of SW:NE wind frequency was 1.1 versus 1.8 for the remaining six hindcast years in which hypoxia initiated preferentially along the Ohio coast in July. The July thermocline was tilted north-south in years with more frequent SW winds. As a result, the simulated and observed hypolimnion was thinner along the Ohio coast where hypoxia initially developed versus a thicker hypolimnion along the Ontario coast. For example, the wind field in 2017 had a stronger southwesterly component than in 2015 (Figure 9). Accordingly, upwelling developed on the north shore and a thin thermocline with earlier initiation of hypoxia along the south shore in 2017, while these features were less prominent in 2015 (Figure 10).

Occasional upwelling events brought hypoxic water to nearshore locations along the Ohio coast, and these events were associated with northeast wind. For example, drinking water plants with nearshore water intakes were affected by hypoxic episodes in August of 2006 (Ruberg et al., 2008), September 2016, and July 2017. Each of these events was preceded by wind from the NE quadrant at speeds >8 m/s lasting at least 24 hr (Figures 11, 12 and 13). Wind from the NE on 1–2 September 2016 preceded an upwelling event that caused the modeled location of the thermocline to move shoreward along the Ohio coast and offshore along the Ontario coast (Figure 11a and 11c and 11e and 11g), which was coincident with observed decrease in temperature and DO at sensors located in the pump stations of drinking water intakes at Mentor and Ashtabula (Figures 11e–11h). A similar event occurred in July 2017, with NE wind >8 m/s on 28–29 July preceding shoreward movement of the modeled thermocline location along the Ohio coast and offshore movement along the Ontario coast (Figures 12a and 12c and 12e and 12g). In 2017, a thermistor string located at a Cleveland water intake (~ 5 km offshore) recorded elevation of the thermocline and decrease in surface temperature, with relatively little change observed at the thermistor string located 25 km offshore of Cleveland or the sensors 10 km from the Ontario coast (Figures 12a and 12c). In addition, a decrease in temperature and DO was observed at Mentor and Ashtabula associated with the event (Figures 12e and 12g and 12f and 12h). Finally, bottom temperature and DO increased at our Sandusky basin mooring, consistent with the model (Figures 12e and 12g and 12f and 12h).

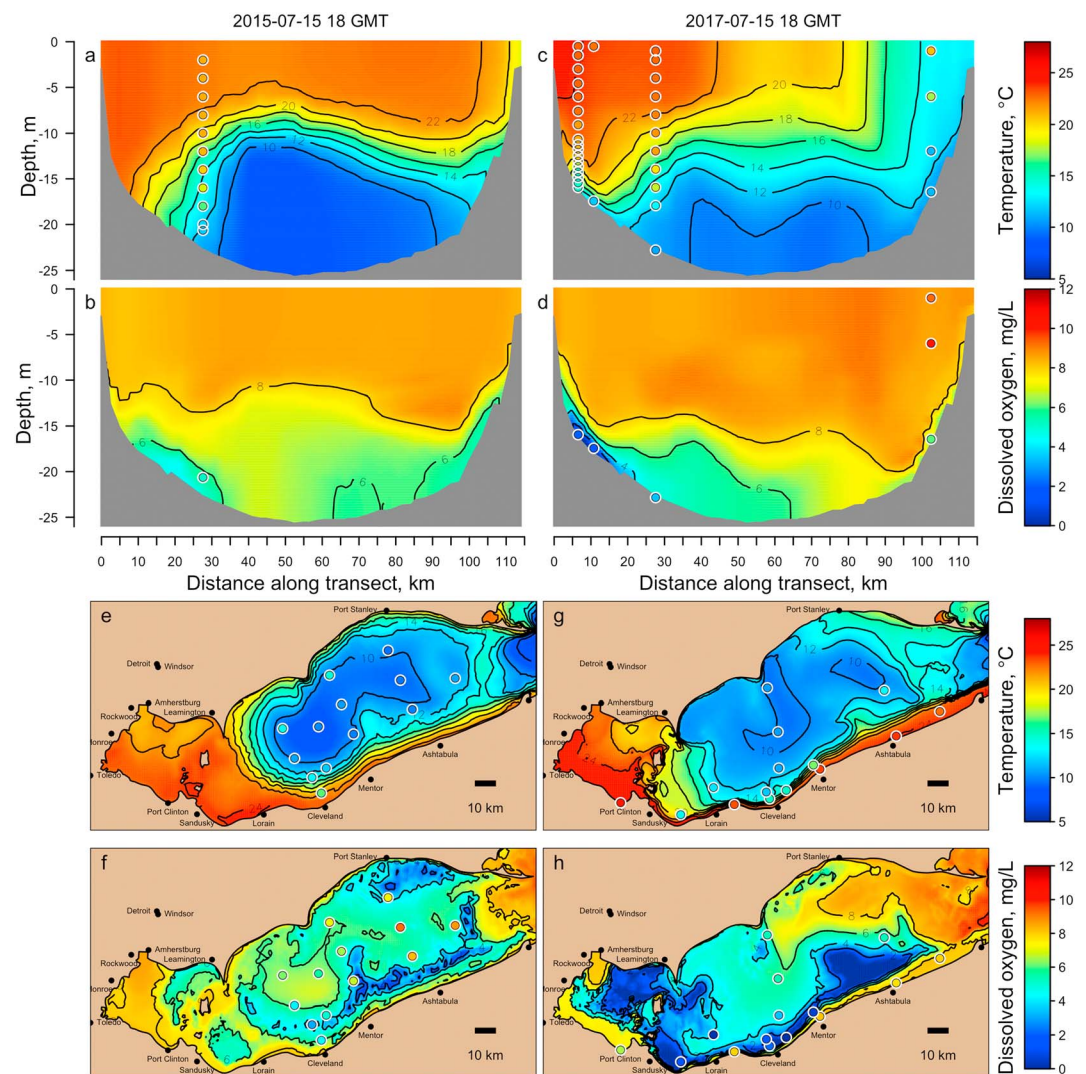


Figure 10. Depiction of earlier initiation of hypoxia along the Ohio coast in 2017 (d, h), a year with a dominant southwesterly wind component in June–July (Figure 9) compared to 2015, a year without a dominant wind component (Figure 9). Model data (color fields and contours) and observations (symbols) are shown on the same color scale. Cross-sectional view (a–d) from Cleveland Ohio to Port Glasgow Ontario (Figure 1) showing temperature and dissolved oxygen. Maps of bottom temperature and dissolved oxygen are (e–h) on the same days.

A goal of model development was to predict upwelling events that caused sudden changes in temperature and water quality at nearshore intakes of drinking water treatment plants. Thus, we evaluated the skill of the model in predicting such events. We defined two types of events: (1) a decrease in temperature $> 3\text{ }^{\circ}\text{C}$ relative to the preceding 24-hr average and (2) DO $< 4\text{ mg/L}$ at a water intake sensor. Low DO in itself is not detrimental to drinking water treatment, but other water-quality variables associated with hypoxia, such as low pH or elevated Fe and Mn trigger adjustments to treatment processes. A value of pH < 7.5 is a threshold for pH adjustment in some drinking water plants: 99% of pH < 7.5 observations occurred with DO $< 5\text{ mg/L}$, 82% with DO $< 4\text{ mg/L}$, and with DO $< 4\text{ mg/L}$ pH < 7.5 occurred 62% of the time (Figure S10). Comparison of modeled to observed time series of temperature and DO at water intake locations showed that the number of events and model skill differed by location (Figures S11 and S12). To assess potential utility of the forecast, we compared model skill to a benchmark representing the next best alternative source of information. Most drinking water plants have a sensor in incoming raw water, which provides the best available information in the absence of a forecast model; thus, we defined a benchmark *persistence* forecast as the assumption of no change from the most recent observed value. The PSS of the persistence forecast is a perfect 1.0 on forecast day 0, by definition, but declines as the assumption of no change is carried into the future

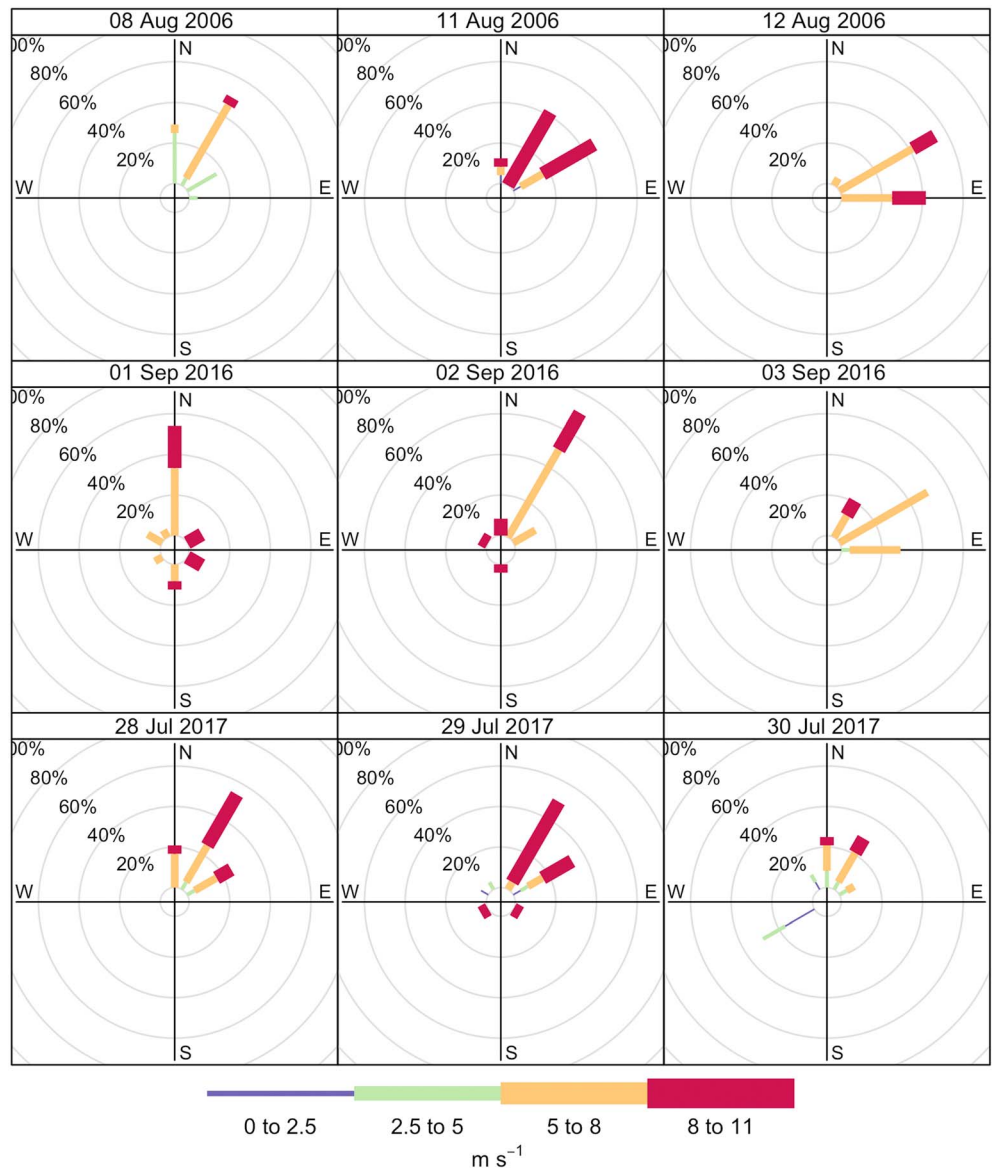


Figure 11. Wind rose plot showing NE wind in days preceding upwelling events along the Ohio coast described by Ruberg et al. (2008) and shown in Figures 12 and 13.

(Figure 14). Forecast skill was limited, but greater than the persistence forecast at day 1 and beyond for temperature events, and day 3 and beyond for DO events, thus indicating that the forecast may provide useful information beyond what can be obtained from real-time sensors.

3.3. Model Sensitivity to Meteorological Forcing

Simulated Lake Erie thermal structure was sensitive to alternate meteorological forcing. HRRR and interpolated meteorological forcing simulated bottom temperature with similar skill, when all daily observations were considered (Table S2; Bias 0.43, 0.48 °C; NS 0.78, 0.78, respectively; Figure S13). However, bottom DO was biased lower for HRRR relative to interpolated (−1.36 vs −0.16 mg/L, respectively; Figure S13). Bias in surface mixed layer thickness was improved with HRRR relative to interpolated (−2.29 m vs −2.83 m, respectively), and bias in hypolimnion thickness was also reduced (0.09 m vs 0.75 m, respectively; Figure S14). Thus, HRRR forcing produced a deeper thermocline than interpolated. When only deep-water stations were considered (USEPA stations >20-m depth), HRRR bottom temperature was biased higher than

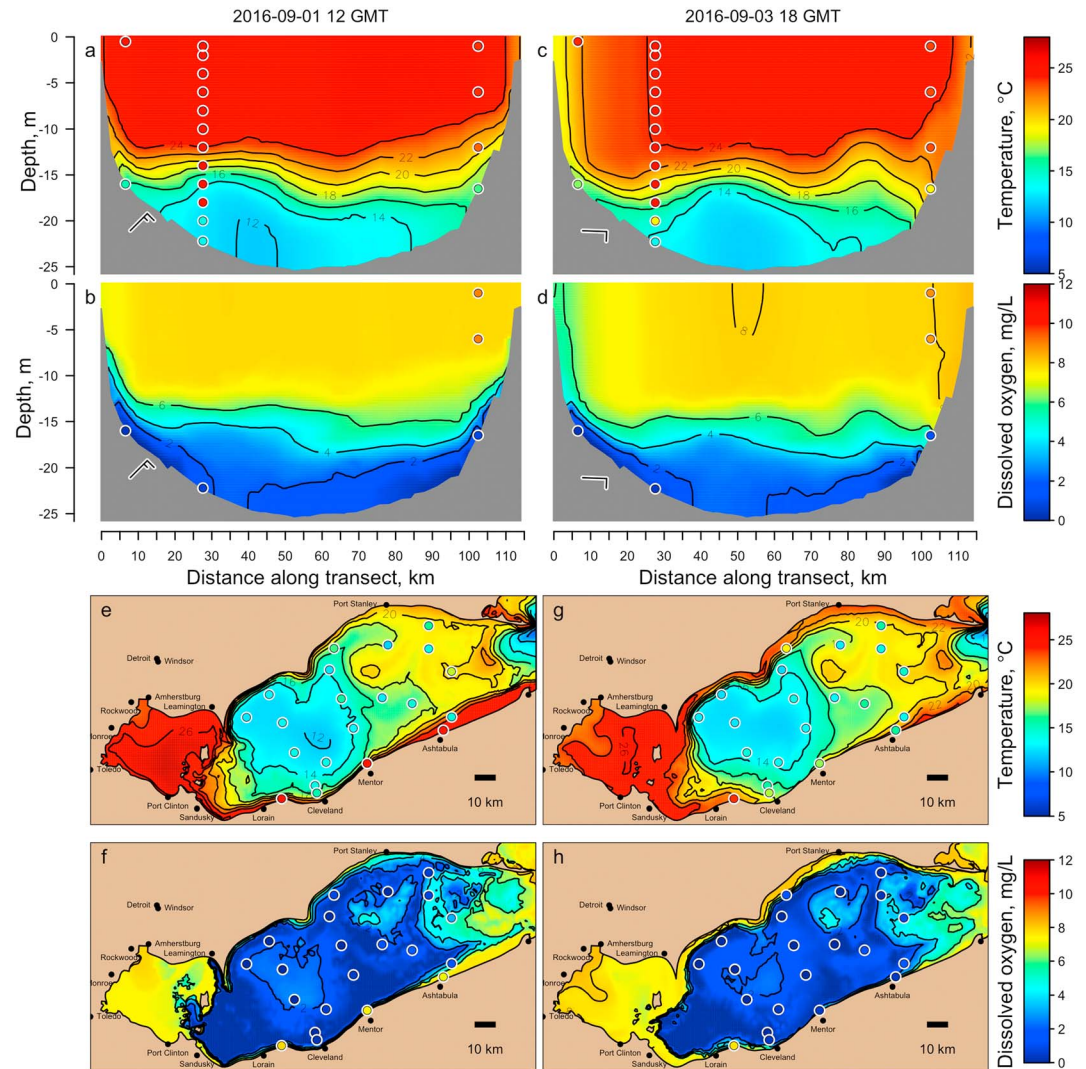


Figure 12. Depiction of an upwelling event along the south coast of the Lake Erie Central basin occurring on 1–3 September 2016 with model data (color fields and contours) and observations (symbols) on the same color scale. Cross-sectional view (a–d) from Cleveland Ohio to Port Glasgow Ontario (Figure 1) showing temperature and dissolved oxygen. Maps of bottom temperature and dissolved oxygen (e–h) are on the same days. Sensors in drinking water intakes at Mentor and Ashtabula recorded a decrease in temperature and dissolved oxygen (e–h).

interpolated (1.34 °C vs 0.27 °C, respectively), but HRRR bottom DO had little bias and greater overall skill than interpolated (Table S2; NS 0.74 vs 0.63, respectively); thus, low-biased bottom DO in HRRR, when all observations were considered, was associated with nearshore stations. The difference in thermocline shape between HRRR and interpolated is illustrated by comparison to a transect of CTD profiles heading offshore from a location near Ashtabula to midlake. Interpolated produced a domed thermocline that was too shallow midlake but more accurately simulated the location where the thermocline intersects the bottom near the coast (Figure 15a vs Figure 15c). In contrast, HRRR simulated thermocline depth and hypolimnion thickness more accurately midlake, but the thermocline nearshore was too shallow, resulting in less accurate temperature and DO nearshore (Figure 15).

4. Discussion

Our spatially detailed model simulated spatial and temporal patterns of hypoxia with moderate skill using a relatively simple, physically based DO model that included temperature-dependent, but otherwise spatially

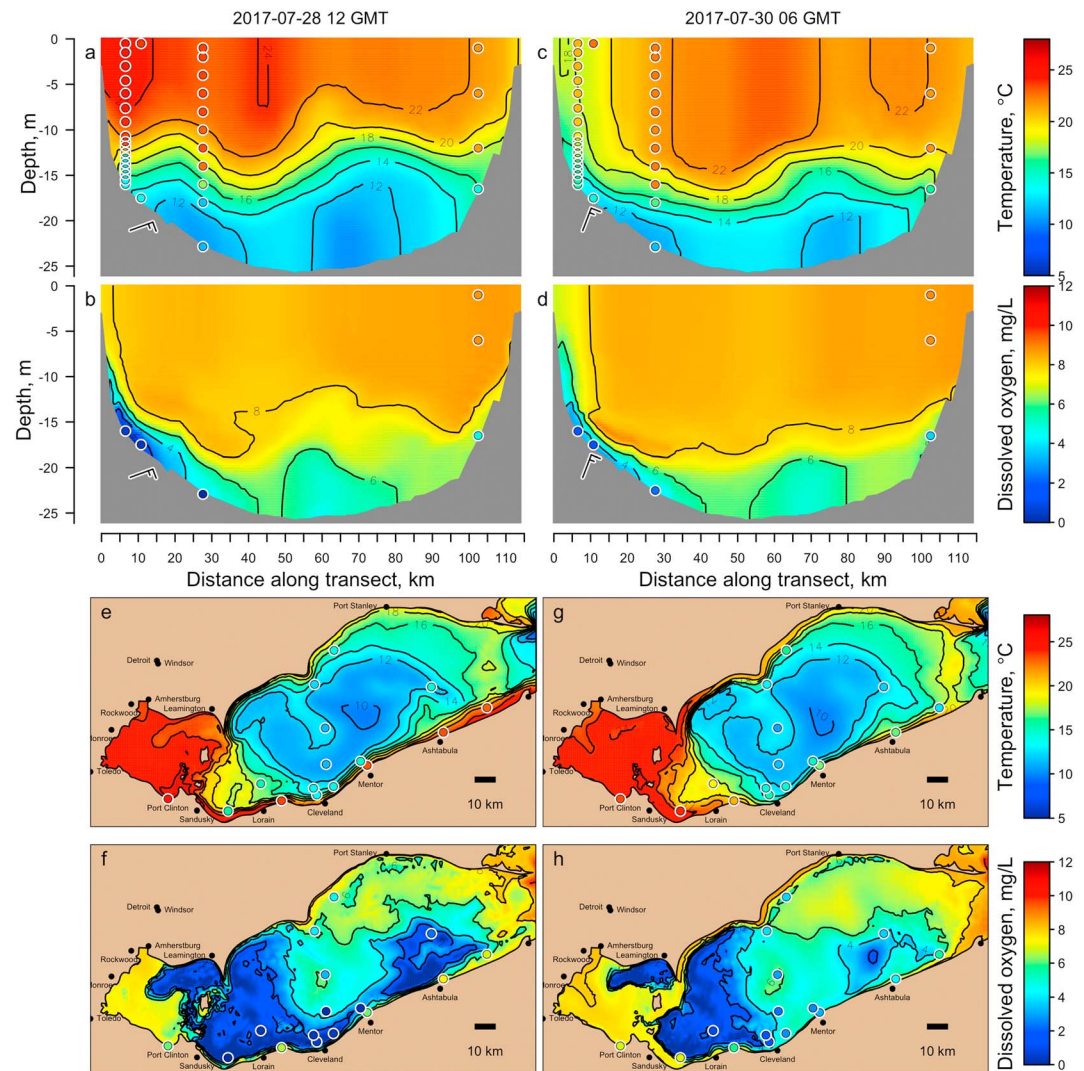


Figure 13. Depiction of an upwelling event along the south coast of the Lake Erie Central basin occurring on 28–30 July 2017 with model data (color fields and contours) and observations (symbols) on the same color scale. Cross-sectional view from Cleveland Ohio to Port Glasgow Ontario (Figure 1) showing temperature and dissolved oxygen. Maps of bottom temperature and dissolved oxygen are (e–h) on the same days. Sensors in drinking water intakes at Avon Lake, Mentor, and Ashtabula recorded a decrease in temperature and dissolved oxygen.

uniform, rates of oxygen demand. Having a large number of observations in nearshore locations provided for a rigorous skill assessment of the model's ability to simulate the shoreward boundary of the hypoxic zone.

Previous Lake Erie hypoxia models have differed in complexity from relatively simple one-dimensional physically based models (Rucinski et al., 2010) to complex models having multiple plankton and nutrient state variables (Bocaniov et al., 2016; Zhang et al., 2008). Stratification of the water column is a prerequisite for hypoxia development, so it is known that physical drivers are influential (Mortimer, 1987), but the ability of a model that neglects autochthonous production of labile organic matter to simulate spatial, seasonal, and interannual variation in Lake Erie hypoxia has not previously been explored in detail. Our model simulated much of the observed spatial and temporal variance in hypoxia, indicating that these patterns are largely physically driven. However, our model exhibited limited skill in some aspects that point to room for further improvement and also provide insights into spatial patterns in sediment oxygen demand. West-to-east bias in simulated bottom DO suggests that there may be a west-east gradient in sediment oxygen demand, driven by the trophic gradient from the eutrophic western basin to the oligotrophic eastern

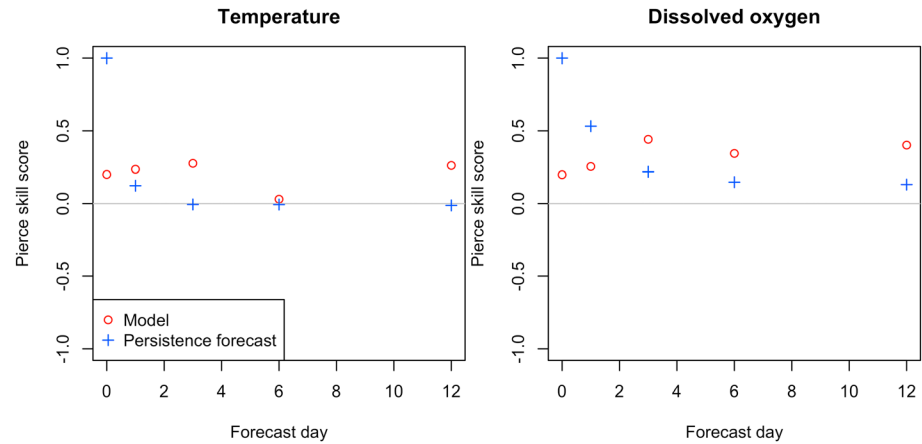


Figure 14. Evaluation of model skill in predicting events at drinking water intakes in Ohio in 2017. Events were defined as (1) a decrease in temperature $> 3^{\circ}\text{C}$ relative to the preceding 24-hr average, and (2) DO $< 4\text{ mg/L}$. Pierce skill score values range from -1.0 to 1.0 , with positive values indicating that the rate of correct prediction of events was greater than the false positive rate. A *persistence* forecast was defined as a benchmark, consisting of carrying the most recent sensor observation forward in time.

basin. Although previous studies have measured and reported rates of sediment oxygen demand in Lake Erie (Matisoff & Neeson, 2005; Schloesser et al., 2005; Snodgrass, 1987), a spatial trend would be challenging to resolve from observations given potential variation at small spatial and temporal scales (e.g., Rao et al., 2008). Studies from the 1960s, reviewed by Mortimer (1987), found that areas with highest sediment organic content in the central basin occurred in the western half and associated this with earlier oxygen depletion there (their Figure 7). Our model predicted frequent hypoxia north of Pelee Island (Figures 1

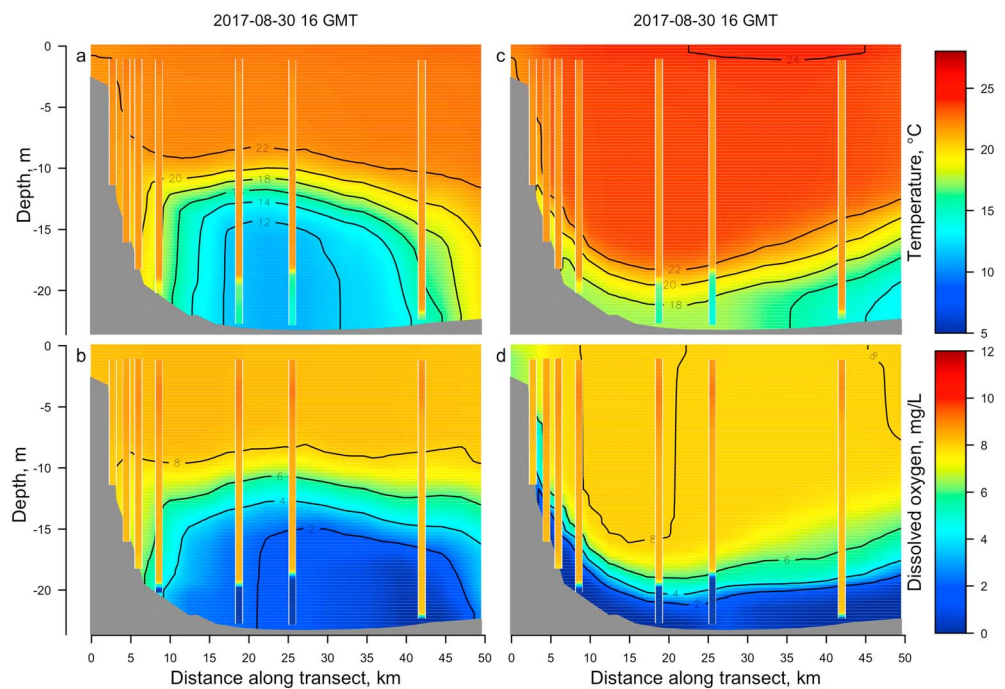


Figure 15. Cross-sectional view of Lake Erie along the Ohio EPA transect heading offshore from a location near Ashtabula to midlake (Figure 1), illustrating the sensitivity of the model thermal structure to alternative sources of meteorological forcing: Interpolated from observations (a, b) or the High-Resolution Rapid Refresh weather forecast model with assimilated observations (c, d). Observations (vertical bands) from CTD profiles were plotted over model data (color fields and contours) on the same color scale. EPA = Environmental Protection Agency; CTD = conductivity, temperature, and depth.

and 3–5), especially in July, but limited observations were available for model assessment in this region. Total phosphorus in the northern western basin is less than in the southern western basin (18.5 vs 39.2 $\mu\text{gP/L}$, respectively, 2000–2015 mean; USEPA data, <https://cdx.epa.gov>, accessed 11-2016). The northern and southern regions of the western basin are influenced by the Detroit River and Maumee River, respectively. Relatively oligotrophic Detroit River water may reduce sediment oxygen demand in the northern western basin; neglecting this effect could have led to overprediction of hypoxia north of Pelee Island in our model. Inclusion of autochthonous production of labile organic matter has the potential to improve simulated spatial patterns of hypoxia, given strong trophic gradients that exist in Lake Erie.

Spatial and seasonal patterns of hypoxia depicted by our model differed from recent depictions of Lake Erie hypoxia but had features in common with earlier studies. For example, Zhou et al. (2013) published spatial depictions of hypoxic area in Lake Erie, based on application of geostatistical kriging to observations collected almost exclusively in the deepest waters of the central basin (> 20 m), and focusing on August, September, and October excluding July. Their analysis depicted hypoxia as limited to deep waters of the central basin and varying mainly in eastward extent from year to year. Their statistical model was not able to predict the occurrence of hypoxia outside of the deepest waters of the central basin because it was calibrated on only deep-water observations. In contrast, our physically based, mechanistic model predicted initiation of hypoxia in July, often preferentially in a narrow band along the Ohio coast, and in relatively shallow areas including the Sandusky basin and north of Pelee Island. In addition, our model simulated episodes of hypoxia affecting nearshore locations, such as water intakes 0.5–1 km from shore, associated with upwelling events. An extensive set of nearshore and deep-water observations collected from multiple investigators confirmed these novel observations. Perello et al. (2017) reported July hypoxia in the Sandusky basin, and we included their observations in our analysis. Studies from the 1960s to 1970s, reviewed by Mortimer (1987), found hypoxia in Sandusky basin (their Figures 6 and 7). Simulated hypoxia north of Pelee Island in our model requires more rigorous confirmation. Previous reports of upwelling events affecting water intakes were limited to isolated incidents (Ruberg et al., 2008), but we report multiple events per season. Occurrences of hypoxia earlier than previously reported (July) and in shallower locations are in contrast to estimates of hypoxic area based mainly on deep-water observations (Zhou et al., 2013). Hypoxic area is a metric for eutrophication management objectives (Great Lakes Water Quality Protocol, 2012; Scavia et al., 2014); our model provides insight into locations within Lake Erie that may be susceptible to hypoxia but missed by monitoring programs.

Previous modeling studies have simulated Lake Erie hypoxia but did not extensively assess simulated spatial patterns relative to observations and did not report preferential initiation of hypoxia along the Ohio coast. For example, a number of models lacked sufficient spatial detail to simulate spatial patterns of hypoxia (Lam & Schertzer, 1987; Rucinski et al., 2010; Zhang et al., 2008). Conversely, Bocaniov et al. (2016) reported initiation of hypoxia north of Pelee Island in July, showed depictions of simulated hypoxia in Sandusky basin, and reported simulated initiation of hypoxia nearshore as a novel finding, but they neither assessed these model predictions with observations nor did they report preferential initiation of hypoxia along the Ohio coast. Mortimer (1987) reported hypoxia surveys in August–September of 1959 and 1960 that found the lowest DO values (< 0.5 mg/L) near the Ohio coast, 10–30 km north of Cleveland (their Figure 6); the same review reported a tilted thermocline with upwelling along the Ontario coast and warmest surface water in the south, associated with frequent W-SW winds, but earlier initiation of hypoxia along the Ohio coast was not directly associated with the deeper thermocline in that location.

We found that relatively frequent southwest winds caused a persistent north-south tilt to the thermocline, resulting in a thinner hypolimnion and earlier initiation of hypoxia along the Ohio coast than further north in most years. Occasional northeast wind events caused upwelling along the Ohio coast, bringing cold and potentially hypoxic, hypolimnetic water to nearshore locations. These observations are consistent with coastal upwelling/downwelling by Ekman transport, as described by others (Csanady, 1977; Rao & Schwab, 2007; Simons & Schertzer, 1987). However, there have been limited reports on the effect of Ekman transport-driven coastal upwelling on persistent and short-term patterns of hypoxia. Rao et al. (2014) reported an upwelling event that resulted in a fish kill and a rapid decrease in temperature, DO, and pH at drinking water intakes on the Ontario coast of the central basin. This event was driven by Ekman transport associated with a west-southwest wind event at 8 m/s. Our observations and simulations documented similar short-term upwelling events driven by northeast winds and Ekman transport on the

Ohio coast. Kraus et al. (2015) monitored DO at 14- to 19-m depth along the Ohio coast and found greater than expected variability at the shallower stations, which they attributed to advection of hypolimnetic water by internal waves. In addition to the short-term events, we documented a persistent downwelling along the Ohio coast that occurred in July of most years, associated with frequent southwest winds. We further associated the persistent downwelling with earlier initiation of hypoxia a few kilometers offshore of the Ohio coast than further north. Müller et al. (2012) identified hypolimnion thickness as a primary predictor of hypoxia onset in eutrophic lakes; a thin hypolimnion is depleted of oxygen more quickly than a thick hypolimnion for given rates of sediment and water column oxygen demand. Local sources of nutrients or labile organic matter could contribute to the observed early initiation of hypoxia along the Ohio coast, but our model simulated this phenomenon with spatially uniform prescribed rates of sediment and water column oxygen demand in the central and western basins, which suggests that the pattern is physically driven by a north-south gradient in hypolimnion thickness.

In addition to episodes of coastal hypoxia caused by upwelling, we documented widespread development of hypoxia in shallow, coastal areas during a period of calm, hot weather in September 2017. Such episodes can be ecologically consequential. Large, burrowing mayflies of the genus *Hexagenia* are an important food for fish and indicator of water and substrate quality in lakes. A single hypoxic episode in the western basin, resulting from a period of hot, calm weather in early September 1953 (Britt, 1955) severely reduced the formerly abundant *Hexagenia* population. Subsequent hypoxic episodes nearly extirpated *Hexagenia* from western Lake Erie in the early 1960s, but the population recovered in the 1990s, responding to improved water quality (Madenjian et al., 1998). *Hexagenia* recruitment success was shown to be negatively impacted by episodes of stratification associated with periods of calm, hot weather, and assumed hypoxia, over the period 1997–2002 (Bridgeman et al., 2006). Our model, combined with an extensive set of nearshore observations, documented the progression of a similar hypoxic event in September 2017, which caused observations of bottom hypoxia not only in the western basin but also in nearshore waters of the central basin. Such episodes highlight that *Hexagenia* populations, and potentially other benthic organisms, may be at risk under present-day water-quality conditions in Lake Erie.

Modeled hypolimnion thickness was highly sensitive to alternative sources of meteorological forcing. Beletsky et al. (2013) similarly found that Lake Erie and Lake Michigan (Beletsky et al., 2003) thermal structure and circulation were sensitive to meteorological forcing, with winds from atmospheric models producing superior results in comparison to interpolated winds. Model-derived winds may have more physically realistic representation of vorticity, while spatial interpolation may result in distorted and unrealistic wind fields over water. Beletsky et al. (2013) found that accurate representation of vorticity in the wind field is necessary to produce the bowl-shaped thermocline that was present in the central basin of Lake Erie, in their observations as well as ours (Figure 15c), through the process of Ekman pumping. Even though HRRR forcing resulted in more accurate simulation of offshore thermal structure in our study, interpolated forcing resulted in more accurate simulation of hypoxia overall because the location where the thermocline intersected the bottom was nearer the coast than observed with HRRR forcing, a critical variable for our hypoxia simulations. It is possible that additional mixing mechanisms should be represented in the model (e.g., wind waves) to produce a deeper surface mixed layer near the coast in our HRRR simulations.

5. Conclusion

We found that hypoxia in Lake Erie often initiates preferentially along the Ohio coast in July, associated with Ekman transport-driven coastal downwelling along the south shore, which produces a thinner hypolimnion in that location. Episodes of coastal upwelling brought hypoxic water to nearshore locations, including drinking water intakes; these events along the Ohio coast were associated with Ekman transport driven by northeast winds 8 m/s. A linked hydrodynamic and physical DO model that included temperature-dependent, but otherwise spatially uniform, rates of oxygen demand had useful but limited skill in reproducing observed spatial and temporal patterns of hypoxia in Lake Erie. Modeled bottom DO exhibited an east-west gradient in mean bias across the central basin, suggesting that the assumption of spatially uniform sediment oxygen demand in the central basin is incorrect. Further research is needed to determine whether higher rates of oxygen demand exist in the western central basin owing to proximity to the eutrophic western basin.

Acknowledgments

This paper is the result of research funded by the National Oceanic and Atmospheric Administration's National Centers for Coastal Ocean Science Competitive Research Program under award NA16NOS4780209 to the University of Michigan and NOAA GLERL. This is CHRP contribution 242. This is Cooperative Institute of Great Lakes Research (CIGLR) contribution 1146 and GLERL contribution 1925. The FVCOM model code is available from <http://fvcom.smast.umassd.edu/>. Steve Ruberg and Steve Constant of NOAA GLERL, and Tom Johengen of CIGLR designed and deployed instrumented moorings. Greg Lang of NOAA GLERL ran the hypoxia nowcast/forecast model. Additional temperature and dissolved oxygen observations were shared by Edward Verhamme of LimnoTech, Scott Winkler of Ohio Environmental Protection Agency, and Todd Howell of Ontario Ministry of the Environment, Conservation and Parks. In addition to sources cited in the text, data are available online: <https://www.glerl.noaa.gov/data/chrp/>.

References

Allan, J. D., Smith, S. D., McIntyre, P. B., Joseph, C. A., Dickinson, C. E., Marino, A. L., et al. (2015). Using cultural ecosystem services to inform restoration priorities in the Laurentian Great Lakes. *Frontiers in Ecology and the Environment*, 13(8), 418–424. <https://doi.org/10.1890/140328>

Anderson, E., Bechle, A. J., Wu, C. H., Schwab, D. J., Mann, G. E., & Lombardy, K. A. (2015). Reconstruction of a meteotsunami in Lake Erie on 27 May 2012: Roles of atmospheric conditions on hydrodynamic response in enclosed basins. *Journal of Geophysical Research: Oceans*, 120, 8020–8038. <https://doi.org/10.1002/2015JC010883>

Anderson, E., Fujisaki-Manome, A., Kessler, J., Lang, G., Chu, P., Kelley, J., et al. (2018). Ice forecasting in the next-Generation Great Lakes Operational Forecast System (GLOFS). *Journal of Marine Science and Engineering*, 6, 123. <https://doi.org/10.3390/jmse6040123>

Anderson, E., & Schwab, D. (2013). Predicting the oscillating bi-directional exchange flow in the Straits of Mackinac. *Journal of Great Lakes Research*, 39(4), 663–671. <https://doi.org/10.1016/j.jglr.2013.09.001>

Anderson, E., Schwab, D. J., & Lang, G. A. (2010). Real-time hydraulic and hydrodynamic model of the St. Clair River, Lake St. Clair, Detroit River System. *Journal of Hydraulic Engineering*, 136(8), 507–518. [https://doi.org/10.1061/\(ASCE\)HY.1943-7900.0000203](https://doi.org/10.1061/(ASCE)HY.1943-7900.0000203)

Arhonditsis, G. B., Adams-VanHarn, B. A., Nielsen, L., Stow, C. A., & Reckhow, K. H. (2006). Evaluation of the current state of mechanistic aquatic biogeochemical modeling: Citation analysis and future perspectives. *Environmental Science & Technology*, 40(21), 6547–6554. <https://doi.org/10.1021/es061030q>

Bai, X., Wang, J., Schwab, D. J., Yang, Y., Luo, L., Leshkevich, G. A., & Liu, S. (2013). Modeling 1993–2008 climatology of seasonal general circulation and thermal structure in the Great Lakes using FVCOM. *Ocean Modelling*, 65, 40–63. <https://doi.org/10.1016/j.ocemod.2013.02.003>

Bartish, T. (1987). A review of exchange processes among the three basins of Lake Erie. *Journal of Great Lakes Research*, 13(4), 607–618. [https://doi.org/10.1016/S0380-1330\(87\)71676-1](https://doi.org/10.1016/S0380-1330(87)71676-1)

Beletsky, D., Hawley, N., & Rao, Y. R. (2013). Modeling summer circulation and thermal structure of Lake Erie. *Journal of Geophysical Research: Oceans*, 118, 6238–6252. <https://doi.org/10.1002/2013JC008854>

Beletsky, D., Hawley, N., Rao, Y. R., Vanderploeg, H. A., Beletsky, R., Schwab, D. J., & Ruberg, S. A. (2012). Summer thermal structure and anticyclonic circulation of Lake Erie. *Geophysical Research Letters*, 39, L06605. <https://doi.org/10.1029/2012GL051002>

Beletsky, D., O'Connor, W. P., Schwab, D. J., & Dietrich, D. E. (1997). Numerical simulation of internal Kelvin waves and coastal upwelling fronts. *Journal of Physical Oceanography*, 27(7), 1197–1215. [https://doi.org/10.1175/1520-0485\(1997\)027<1197:NSOIKW>2.0.CO;2](https://doi.org/10.1175/1520-0485(1997)027<1197:NSOIKW>2.0.CO;2)

Beletsky, D., Schwab, D., & McCormick, M. (2006). Modeling the 1998–2003 summer circulation and thermal structure in Lake Michigan. *Journal of Geophysical Research*, 111, C10010. <https://doi.org/10.1029/2005JC003222>

Beletsky, D., Schwab, D., Roebber, P., McCormick, M., Miller, G., & Saylor, J. (2003). Modeling wind-driven circulation during the March 1998 sediment resuspension event in Lake Michigan. *Journal of Geophysical Research*, 108(C2), 3038. <https://doi.org/10.1029/2001JC001159>

Benjamin, S. G., Weygandt, S. S., Brown, J. M., Hu, M., Alexander, C. R., Smirnova, T. G., et al. (2016). A North American hourly assimilation and model forecast cycle: The Rapid Refresh. *Monthly Weather Review*, 144(4), 1669–1694. <https://doi.org/10.1175/MWR-D-15-0242.1>

Bever, A. J., Friedrichs, M. A., Friedrichs, C. T., Scully, M. E., & Lanerolle, L. W. (2013). Combining observations and numerical model results to improve estimates of hypoxic volume within the Chesapeake Bay, USA. *Journal of Geophysical Research: Oceans*, 118, 4924–4944. <https://doi.org/10.1002/jgrc.20331>

Bocaniov, S. A., Leon, L. F., Rao, Y. R., Schwab, D. J., & Scavia, D. (2016). Simulating the effect of nutrient reduction on hypoxia in a large lake (Lake Erie, USA-Canada) with a three-dimensional lake model. *Journal of Great Lakes Research*, 42, 1228–1240. <https://doi.org/10.1016/j.jglr.2016.06.001>

Bouffard, D., Boegman, L., & Rao, Y. R. (2012). Poincaré wave-induced mixing in a large lake. *Limnology and Oceanography*, 57, 1201–1216. <https://doi.org/10.4319/lo.2012.57.4.1201>

Bridgeman, T. B., Schloesser, D. W., & Krause, A. E. (2006). Recruitment of *Hexagenia* mayfly nymphs in western Lake Erie linked to environmental variability. *Ecological Applications*, 16, 601–611. [https://doi.org/10.1890/1051-0761\(2006\)016\[0601:ROHMNI\]2.0.CO;2](https://doi.org/10.1890/1051-0761(2006)016[0601:ROHMNI]2.0.CO;2)

Britt, N. W. (1955). Stratification in western Lake Erie in summer of 1953: Effects on the *Hexagenia* (Ephemeroptera) population. *Ecology*, 36(2), 239–244. <https://doi.org/10.2307/1933229>

Burns, N. (1976). Oxygen depletion in the central and eastern basins of Lake Erie, 1970. *Journal of the Fisheries Board of Canada*, 33(3), 512–519. <https://doi.org/10.1139/f76-069>

Cerco, C. F., and Noel, M. R. (2004). The 2002 Chesapeake Bay eutrophication model Rep, 374 pp, U.S. Army Corps of Engineers, U.S. Environmental Protection Agency, EPA 903-R-04-004.

Chapra, S. C. (1997). *Surface water-quality modeling*, (1st ed.p. 844). New York City: McGraw-Hill Co.

Chen, C., Beardsley, R. C., Cowles, G., Qi, J., Lai, Z., Gao, G., et al. (2013). An unstructured grid, finite-volume community ocean model FVCOM user manual (Rep., 416 pp.). University of Massachusetts-Dartmouth, New Bedford, MA. <http://fvcom.smast.umassd.edu/>

Chen, C., Liu, H., & Beardsley, R. C. (2003). An unstructured grid, finite-volume, three-dimensional, primitive equations ocean model: Application to coastal ocean and estuaries. *Journal of Atmospheric and Oceanic Technology*, 20(1), 159–186. [https://doi.org/10.1175/1520-0426\(2003\)020<0159:AUGFVT>2.0.CO;2](https://doi.org/10.1175/1520-0426(2003)020<0159:AUGFVT>2.0.CO;2)

Csanady, G. (1977). Intermittent ‘full’ upwelling in Lake Ontario. *Journal of Geophysical Research*, 82(3), 397–419. <https://doi.org/10.1029/JC082i003p00397>

Csanady, G. (1984). *Circulation in the coastal ocean*. Boston: D. Reidel Publishing Co.

Galperin, B., Kantha, L., Hassid, S., & Rosati, A. (1988). A quasi-equilibrium turbulent energy model for geophysical flows. *Journal of the Atmospheric Sciences*, 45(1), 55–62. [https://doi.org/10.1175/1520-0469\(1988\)045<0055:AQETEM>2.0.CO;2](https://doi.org/10.1175/1520-0469(1988)045<0055:AQETEM>2.0.CO;2)

Great Lakes Water Quality Protocol (2012), Protocol amending the agreement between the United States of America and Canada on Great Lakes water quality. International Joint Commission. http://www.ijc.org/en/Great_Lakes_Water_Quality_Rep., 55 pp, Windsor, Canada.

Greenberg, A. E., Clesceri, L. S., & Eaton, A. D. (1989). *Standard methods for the examination of water and wastewater*, (p. 1100). American Water Works Association: American Public Health Association.

Higashino, M. (2011). Oxygen consumption by a sediment bed for stagnant water: Comparison to SOD with fluid flow. *Water Research*, 45(15), 4381–4389. <https://doi.org/10.1016/j.watres.2011.04.051>

Hogan, R. J., & Mason, I. B. (2012). Deterministic forecasts of binary events. In *Forecast Verification: A Practitioner's Guide in Atmospheric Science*, (Second ed.pp. 31–59). Chichester: Wiley.

- Jabbari, A., Ackerman, J. D., Boegman, L., & Zhao, Y. (2019). Episodic hypoxia in the western basin of Lake Erie. *Limnology and Oceanography*, *00*, 1–17. <https://doi.org/10.1002/lno.11180>
- Ji, R., Davis, C., Chen, C., & Beardsley, R. (2008). Influence of local and external processes on the annual nitrogen cycle and primary productivity on Georges Bank: A 3-D biological–physical modeling study. *Journal of Marine Systems*, *73*(1-2), 31–47. <https://doi.org/10.1016/j.jmarsys.2007.08.002>
- Johnson, M. (2010). A numerical scheme to calculate temperature and salinity dependent air-water transfer velocities for any gas. *Ocean Science*, *6*(4), 913–932. <https://doi.org/10.5194/os-6-913-2010>
- Kelley, J. G. W., Chen, Y., Anderson, E., Lang, G., and Xu, J. (2018). Upgrade of NOS Lake Erie Operational Forecast System (LEOFS) to FVCOM: Model development and hindcast skill assessment. NOAA Technical Memorandum NOS CS 40. https://repository.library.noaa.gov/view/noaa/17253/noaa_17253_DS1.pdf
- Kraus, R. T., Knight, C. T., Farmer, T. M., Gorman, A. M., Collingsworth, P. D., Warren, G. J., et al. (2015). Dynamic hypoxic zones in Lake Erie compress fish habitat, altering vulnerability to fishing gears. *Canadian Journal of Fisheries and Aquatic Sciences*, *72*(6), 797–806. <https://doi.org/10.1139/cjfas-2014-0517>
- Lam, D., & Schertzer, W. (1987). Lake Erie thermocline model results: comparison with 1967–1982 data and relation to anoxic occurrences. *Journal of Great Lakes Research*, *13*(4), 757–769. [https://doi.org/10.1016/S0380-1330\(87\)71689-X](https://doi.org/10.1016/S0380-1330(87)71689-X)
- Li, Y., Li, M., & Kemp, W. M. (2015). A budget analysis of bottom-water dissolved oxygen in Chesapeake Bay. *Estuaries and Coasts*, *38*(6), 2132–2148. <https://doi.org/10.1007/s12237-014-9928-9>
- Madenjian, C. P., Schloesser, D. W., & Krieger, K. A. (1998). Population models of burrowing mayfly recolonization in western Lake Erie. *Ecological Applications*, *8*(4), 1206–1212. [https://doi.org/10.1890/1051-0761\(1998\)008\[1206:PMOBBMR\]2.0.CO;2](https://doi.org/10.1890/1051-0761(1998)008[1206:PMOBBMR]2.0.CO;2)
- Matisoff, G., & Neeson, T. M. (2005). Oxygen concentration and demand in Lake Erie sediments. *Journal of Great Lakes Research*, *31*, 284–295. [https://doi.org/10.1016/S0380-1330\(05\)70321-X](https://doi.org/10.1016/S0380-1330(05)70321-X)
- Mortimer, C. (1987). Fifty years of physical investigations and related limnological studies on Lake Erie, 1928–1977. *Journal of Great Lakes Research*, *13*(4), 407–435. [https://doi.org/10.1016/S0380-1330\(87\)71664-5](https://doi.org/10.1016/S0380-1330(87)71664-5)
- Müller, B., Bryant, L. D., Matzinger, A., & Wüest, A. (2012). Hypolimnetic oxygen depletion in eutrophic lakes. *Environmental Science & Technology*, *46*(18), 9964–9971. <https://doi.org/10.1021/es301422r>
- Perello, M. M., Kane, D. D., Golnick, P., Hughes, M. C., Thomas, M. A., & Conroy, J. D. (2017). Effects of local weather variation on water-column stratification and hypoxia in the western, Sandusky, and central basins of Lake Erie. *Water*, *9*(4), 279. <https://doi.org/10.3390/w9040279>
- Rao, Y. R., Hawley, N., Charlton, M. N., & Schertzer, W. M. (2008). Physical processes and hypoxia in the central basin of Lake Erie. *Limnology and Oceanography*, *53*(5), 2007–2020. <https://doi.org/10.4319/lo.2008.53.5.2007>
- Rao, Y. R., Howell, T., Watson, S. B., & Abernethy, S. (2014). On hypoxia and fish kills along the north shore of Lake Erie. *Journal of Great Lakes Research*, *40*(1), 187–191. <https://doi.org/10.1016/j.jglr.2013.11.007>
- Rao, Y. R., & Schwab, D. J. (2007). Transport and mixing between the coastal and offshore waters in the Great Lakes: A review. *Journal of Great Lakes Research*, *33*(1), 202–218. [https://doi.org/10.3394/0380-1330\(2007\)33\[202:TAMBTC\]2.0.CO;2](https://doi.org/10.3394/0380-1330(2007)33[202:TAMBTC]2.0.CO;2)
- Robson, B. J. (2014). When do aquatic systems models provide useful predictions, what is changing, and what is next? *Environmental Modelling & Software*, *61*, 287–296. <https://doi.org/10.1016/j.envsoft.2014.01.009>
- Rodrigues, R. R., & Lorenzetti, J. A. (2001). A numerical study of the effects of bottom topography and coastline geometry on the Southeast Brazilian coastal upwelling. *Continental Shelf Research*, *21*(4), 371–394. [https://doi.org/10.1016/S0278-4343\(00\)00094-7](https://doi.org/10.1016/S0278-4343(00)00094-7)
- Ruberg, S. A., Guasp, E., Hawley, N., Muzzi, R. W., Brandt, S. B., Vanderploeg, H. A., et al. (2008). Societal benefits of the Real-time Coastal Observation Network (ReCON): Implications for municipal drinking water quality. *Marine Technology Society Journal*, *42*(3), 103–109. <https://doi.org/10.4031/002533208786842471>
- Rucinski, D. K., Beletsky, D., DePinto, J. V., Schwab, D. J., & Scavia, D. (2010). A simple 1-dimensional, climate based dissolved oxygen model for the central basin of Lake Erie. *Journal of Great Lakes Research*, *36*(3), 465–476. <https://doi.org/10.1016/j.jglr.2010.06.002>
- Scavia, D., Allan, J. D., Arend, K. K., Bartell, S., Beletsky, D., Bosch, N. S., et al. (2014). Assessing and addressing the re-eutrophication of Lake Erie: Central basin hypoxia. *Journal of Great Lakes Research*, *40*(2), 226–246. <https://doi.org/10.1016/j.jglr.2014.02.004>
- Schloesser, D. W., Stickel, R. G., & Bridgeman, T. B. (2005). Potential oxygen demand of sediments from Lake Erie. *Journal of Great Lakes Research*, *31*, 272–283. [https://doi.org/10.1016/S0380-1330\(05\)70320-8](https://doi.org/10.1016/S0380-1330(05)70320-8)
- Schwab, D. J., and Beletsky, D. (1998). Lake Michigan mass balance study: Hydrodynamic modeling project Rep, 53 pp, ERL GLERL-108, NOAA GLERL, Ann Arbor, MI.
- Scully, M. E. (2013). Physical controls on hypoxia in Chesapeake Bay: A numerical modeling study. *Journal of Geophysical Research: Oceans*, *118*, 1239–1256. <https://doi.org/10.1002/jgrc.20138>
- Simons, T. J., & Schertzer, W. M. (1987). Stratification, currents, and upwelling in Lake Ontario, summer 1982. *Canadian Journal of Fisheries and Aquatic Sciences*, *44*(12), 2047–2058. <https://doi.org/10.1139/f87-254>
- Smagorinsky, J. (1963). General circulation experiments with the primitive equations: I. The basic experiment. *Monthly Weather Review*, *91*(3), 99–164. [https://doi.org/10.1175/1520-0493\(1963\)091<0099:GCEWTP>2.3.CO;2](https://doi.org/10.1175/1520-0493(1963)091<0099:GCEWTP>2.3.CO;2)
- Snodgrass, W. J. (1987). Analysis of models and measurements for sediment oxygen demand in Lake Erie. *Journal of Great Lakes Research*, *13*(4), 738–756. [https://doi.org/10.1016/S0380-1330\(87\)71688-8](https://doi.org/10.1016/S0380-1330(87)71688-8)
- Stow, C. A., Jolliff, J., McGillicuddy, D. J., Doney, S. C., Allen, J., Friedrichs, M. A. M., et al. (2009). Skill assessment for coupled biological/physical models of marine systems. *Journal of Marine Systems*, *76*(1-2), 4–15. <https://doi.org/10.1016/j.jmarsys.2008.03.011>
- Wang, D., Gouhier, T. C., Menge, B. A., & Ganguly, A. R. (2015). Intensification and spatial homogenization of coastal upwelling under climate change. *Nature*, *518*(7539), 390–394. <https://doi.org/10.1038/nature14235>
- Wanninkhof, R., Asher, W. E., Ho, D. T., Sweeney, C., & McGillis, W. R. (2009). Advances in quantifying air-sea gas exchange and environmental forcing. *Annual Review of Marine Science*, *1*(1), 213–244. <https://doi.org/10.1146/annurev.marine.010908.163742>
- Watson, S. B., Miller, C., Arhonditsis, G., Boyer, G. L., Carmichael, W., Charlton, M. N., et al. (2016). The re-eutrophication of Lake Erie: Harmful algal blooms and hypoxia. *Harmful Algae*, *56*, 44–66. <https://doi.org/10.1016/j.hal.2016.04.010>
- Zhang, H., Culver, D. A., & Boegman, L. (2008). A two-dimensional ecological model of Lake Erie: Application to estimate dreissenid impacts on large lake plankton populations. *Ecological Modelling*, *214*(2-4), 219–241. <https://doi.org/10.1016/j.ecolmodel.2008.02.005>
- Zhou, Y., Obenour, D. R., Scavia, D., Johengen, T. H., & Michalak, A. M. (2013). Spatial and temporal trends in Lake Erie hypoxia, 1987–2007. *Environmental Science & Technology*, *47*(2), 899–905. <https://doi.org/10.1021/es303401b>